Modelling Porcine NAFLD by Deletion of Leptin and defining the role of AMPK in hepatic fibrosis

Tan Tan[1,2, #], Zhiyuan Song[1, #], Runming Wang[1], Shuheng Jiang[3], Zuoxiang Liang[1], Qi Wang[1], Xiaoxiang Hu[1,4], Ning Li[1], and Yiming Xing[1*]

1. State Key Laboratory for Agrobiotechnology, College of Biological Science, China Agricultural University, Beijing, P.R. China.

2. Development Center of Science and Technology, Ministry of Agriculture and Rural Affairs, Beijing, P.R. China.

3. State Key Laboratory of Oncogenes and Related Genes, Shanghai Cancer Institute, Ren Ji Hospital, School of Medicine, Shanghai Jiao Tong University, Shanghai, P.R. China.

4. National Engineering Laboratory for Animal Breeding, China Agricultural University, Beijing, China

# These authors contribute equally to this work.

* Correspondence: ymxing@cau.edu.cn (Y. Xing)

Abstract

Liver fibrosis occurs during chronic liver disease. Advanced liver fibrosis results in cirrhosis, liver failure and often requires liver transplantation. However, due to the lack of human models, mechanisms underlining the pathogenesis of liver fibrosis remain unclear. Recent studies implicated a central role of deranged lipid metabolism in its pathogenesis. In this study, we generated LEPTIN-deficient (*LEPTIN*$^{-/-}$) pigs using zinc finger nuclease technology to investigate the mechanisms of liver fibrosis associated with obesity. The *LEPTIN*$^{-/-}$ pigs showed increased body fat and significant

insulin resistance by 12 months of age. To resemble non-alcoholic fatty liver disease (NAFLD) patients, *LEPTIN*$^{-/-}$ pig developed the phenotypic features of fatty liver, non-alcoholic steatohepatitis (NASH) and hepatic fibrosis with age. Meanwhile, LEPTIN absence reduced phosphorylation of JAK2-STAT3 and AMPK. The alteration of JAK2-STAT3 enhanced fatty acid β-oxidation, whereas inactivation of AMPK led to mitochondrial autophagy, and both contributed to increased oxidative stress in hepatocytes. Although Leptin deletion in the rat liver altered JAK2-STAT3 phosphorylation, it activated the AMPK pathway and prevented liver fibrogenesis in contrast with the *LEPTIN*$^{-/-}$ pig. To our knowledge, the *LEPTIN*$^{-/-}$ pig provides the first model recapitulating the full pathogenesis of NAFLD and its progression toward liver fibrosis. The activity of AMPK signaling pathway suggests a potential target for development of new strategies for the diagnosis and treatment of NAFLD.

Key Words: Liver Fibrosis; LEPTIN; Pig; NAFLD; AMPK pathway

Introduction

Liver fibrosis is a common result of chronic damage to the liver caused by the accumulation of extracellular matrix proteins. A number of liver diseases as well as side effects of some drugs lead to liver fibrosis. Among these causes, non-alcoholic steatohepatitis (NASH) has been recognized as a major etiology (1). It is considered part of the spectrum of non-alcoholic fatty liver disease (NAFLD) (2). Excessive adipose tissue in NAFLD patients leads to an inflammatory state targeting liver

parenchyma with steatosis and fibrosis observed in a significant portion of cases. Hepatic fibrogenesis can progress to cirrhosis which enhances the risk of hepatocellular carcinoma. Alarmingly, few effective pharmacotherapeutic approaches are currently available to block or attenuate development and progression of NAFLD. Liver transplantation is the only efficient treatment option in patients with decompensated cirrhosis (3). Nowadays, the fibrosis stage is viewed as the most important predictor of mortality in NAFLD. However, it is not a unidirectional progressive process, ultimately leading to liver cirrhosis and organ failure, but is in principle reversible. Accordingly, better understanding of mechanisms underlying fibrogenesis are crucial for the development of new strategies for the prevention and treatment of NAFLD and other related liver disease.

Although the pathogenesis of liver fibrosis has not been fully discovered, the primary role is played by the deposition of triglycerides in liver cells and the formation of lipid droplets (4). An accumulation of fatty liver leads to insulin resistance in adipose tissue with increased pro-inflammatory cytokines, which initiate the necrosis and apoptosis of liver cells (5). Elevated free fatty acid (FFA) aggravates the oxidative damage of liver cells, and also leads to insulin resistance. Insulin resistance worsens adipocyte function and promotes the transition of NASH to overt liver fibrosis (6). Although the mechanism of fibrosis deposition has been identified, there are almost no therapies currently available that directly prevent or reverse it. While animal models have been indispensable in further studies, current models possess important limitations which

largely restricted the understanding of the underlying mechanism driving fibrosis development and discovery of new diagnostics and therapeutics for NAFLD and other liver disease.

Leptin and its receptor play an important role in driving the formation of liver fibrosis. Leptin is an adipocyte-derived hormone that mediates energy homeostasis in various ways, including regulating energy metabolism, promoting oxidation of FFAs and inhibiting fat synthesis (7). A substantial subset of obese patients have relatively low circulating levels of Leptin. Leptin-deficient (*ob/ob*) mice and Leptin receptor-deficient (Zucker) rats are widely used for studying the mechanisms underlying the role of Leptin in hepatic fibrosis. However, these models only represent fatty liver, but not fibrosis in the spontaneous state. Although compounds such as thioacetamide or carbon tetrachloromethane have been shown to behave as potent hepatotoxins which trigger hepatic injury and lead to development of fibrosis, these models cannot fully reflect the unembellished transformation of steatohepatitis to fibrosis in NAFLD patients, either in disease spectrum or etiology (8, 9).

This study aimed to investigate the mechanisms of liver fibrosis and NAFLD caused by Leptin deficiency. Due to the high similarity in physiology and metabolism between humans and pigs, we generated the *LEPTIN*$^{-/-}$ pig, which simulates the progression of liver injury, from fatty liver to NASH and hepatic fibrosis, the general physiological alterations and the pathological patterns of NAFLD patients. Compared

89 with *Leptin*$^{-/-}$ rats, we discovered that the alteration of JAK2-STAT3 and AMPK
90 signaling pathways mediates β-oxidation and mitochondrial autophagy respectively in
91 *LEPTIN*$^{-/-}$ pigs, which in turn enhanced oxidative stress and promoted the
92 development of fatty liver to fibrosis. The *LEPTIN*$^{-/-}$ pig model provides a valuable
93 tool to discover the mechanism of the progression of hepatic fibrosis. Meanwhile, the
94 activity of AMPK signaling pathway suggests a potential target to develop new
95 strategy for the diagnosis and treatment of NAFLD.
96
97 **Results**
98 **LEPTIN deletion in pigs causes obesity**
99 To generate LEPTIN-knockout pigs, exon 2 of the porcine *LEPTIN* gene was targeted
100 using ZFNs vectors (Figure 1-figure supplement 1A&B). The mutant pig fetal
101 fibroblasts cell clones were screened and transplanted using somatic cell nuclear
102 transfer to generate transgenic pigs. Through DNA sequencing, various mutants were
103 identified in the transgenic pigs (Figure 1-figure supplement 1C&D). As a matter of
104 convenience, mutants were grouped as *LEPTIN*$^{-/-}$ and *LEPTIN*$^{+/-}$. The expression of
105 *LEPTIN* were nearly undetectable in *LEPTIN*$^{-/-}$ subcutaneous and visceral fat (Figure
106 1- figure supplement 2A). The LEPTIN protein was not detected in *LEPTIN*$^{-/-}$ serum
107 (Figure 1- figure supplement 2B). In order to determine whether the ZFNs resulted in
108 off-target mutations, the genomic regions with the highest levels of homology were
109 analyzed. No off-target mutations were observed at any of the sites profiled using
110 PCR amplification and sequencing (Table S1).

Multiple studies have observed that Leptin plays an important role in the development of obesity. The *LEPTIN*$^{-/-}$ pigs obtained nearly twice the body weight vs control pigs at 21-months of age (103.75 ± 12.37 kg vs 56.50 ± 8.49 kg) (Figure 1A&B). By MSCT, both subcutaneous and abdominal visceral fat were significantly increased in *LEPTIN*$^{-/-}$ compared to control pigs (Figure 1C), and the maximum thickness of subcutaneous fat and the percentage of body fat were more than three times that of control pigs (Figure 1- figure supplement 3A). Using H&E staining *LEPTIN*$^{-/-}$ adipocytes also showed increased volumes (Figure 1- figure supplement 3B).

In order to determine whether LEPTIN deficiency altered clinical indicators of liver disease as observed in obese patients, blood was collected from pigs at 4-, 12- and 18-months of age. Compared to control pigs, the concentration of glucose, triglycerides, total cholesterol and low density lipoprotein (LDL) were significantly increased, while high density lipoprotein (HDL) was reduced in *LEPTIN*$^{-/-}$ serum at the 12-month and 18-month time points (Figure 1 D & Figure 1- figure supplement 3C). The tendency of these blood tests is similar to that of obese patients which indicate that *LEPTIN*$^{-/-}$ pigs demonstrate clinical signs of obesity by 12-months of age.

LEPTIN deletion in pigs causes type II diabetes

Obesity is one of the main factors contributing to type II diabetes in humans.

Consistent with the observed increase in obesity, insulin levels in *LEPTIN*$^{-/-}$ pigs were significantly increased at 12- and 18-months of age (Figure 1E). By applying HOMAs to identify diabetic pigs, the insulin and blood glucose parameters indicated that the *LEPTIN*$^{-/-}$ pigs were insulin resistance by 12-months of age, with reduced insulin sensitivity and islet β cell function (Figure 1F & Figure 1- figure supplement 4A). Histological analysis demonstrated that the size of *LEPTIN*$^{-/-}$ islets and the number of islet β cell were also increased (Figure 1- figure supplement 4B).

Abnormal glucose metabolism is an essential feature of type II diabetes mellitus patients. Thus IVGTT was conducted to determine the pig's ability to regulate blood glucose. Following the injection of highly concentrated glucose, the glucose concentration in *LEPTIN*$^{-/-}$ pigs instantaneously increased to almost 20mmol/L in 10 minutes, which was significantly higher than WT pigs. By 90 minutes post injection, the blood glucose concentration in *LEPTIN*$^{-/-}$ pigs was still higher than initial levels (10mmol/L), whereas the WT pigs were nearly fully recovered (Figure 1G). Thus, the lack of LEPTIN negatively affects insulin mediated glucose metabolism, further obstructing glucose regulation and contributing to type II diabetes.

LEPTIN deletion in pigs results in NAFLD

The incidence rate of non-alcoholic liver injury in obese patients is as high as 90% (12). By the age of 0-6 months, the H&E staining and oil red O staining results showed no visible morphological differences between *LEPTIN*$^{-/-}$ and WT livers

(normal/total individuals=3/3, 100%) (Figure 2A). However, by the age of 6-12 months, the lipid deposition and hepatocyte steatosis in *LEPTIN*$^{-/-}$ pig livers increased (injured/total individuals=3/5, 60%) (Figure 2B). In addition, the triglycerides and the expression of FFA synthesis related genes (*FABP1*, *FASN*, *ELOVL6*, *SCD1* and *PPARA*) were increased significantly in *LEPTIN*$^{-/-}$ pigs (Figure 3A&B). H&E and PAS staining of *LEPTIN*$^{-/-}$ pig livers at 12-22 months of age revealed features of early stage fatty liver disease; whereas the hepatocytes demonstrated obvious balloon degeneration and vacuolated necrosis consistent with middle and late stages. In addition, a large number of mononuclear cells infiltrated the hepatic lobule portal area and between the hepatic parenchymal cells of hepatic lobules. The PAS assay showed carbohydrate components accumulated in *LEPTIN*$^{-/-}$ pig livers (Figure 2C). Real-time PCR results confirmed the expression of *TNFA*, *IL6, NFKB, IL1B* and *MCP1*, a series of cytokines, were significantly up-regulated in the *LEPTIN*$^{-/-}$ pig liver (Figure 3C). IL-1β, TNF-α and IL6 serum concentrations were also significantly increased (damaged individuals/total individuals=2/6, 33%) (Figure 3D).

Liver fibrosis, classified as the third stage of non-alcoholic liver injury, is the last step of the reversible damage process observed clinically. *LEPTIN*$^{-/-}$ pig livers obtained from animals between 22 to 35 months of age demonstrated a high degree of hepatomegaly with the presence of surface fiber bundles and granule (Figure 2D). H&E staining demonstrated that the overall lobule structure was disorganized, and the fibrous septum of the portal area was significantly widened with distinct bridging

177 lesions occurring in the portal and central vein areas in *LEPTIN*$^{-/-}$ pig livers (Figure
178 2D & Figure 3E). Meanwhile, Sirius Red staining revealed collagen accumulation
179 around the hepatic lobule sinus and veins in *LEPTIN*$^{-/-}$ pig livers (damaged
180 individuals/total individuals=3/7, 42.9%) (Figure 2D). Immunofluorescence staining
181 demonstrated that the expression of α-SMA, a marker of fibrosis, was significantly
182 up-regulated in *LEPTIN*$^{-/-}$ livers (Figure 3E). In the clinical diagnosis of liver fibrosis,
183 blood indexes are used to stage the disease. In this study, the fasting blood samples
184 were collected from *LEPTIN*$^{-/-}$ and WT pigs. The results showed that ALT and AST
185 levels in *LEPTIN*$^{-/-}$ blood were greatly increased, indicating significant liver damage.
186 However, comparing with WT, the level of ALP remained unchanged (Figure 3F).
187 The levels of HA and PCIIINP in *LEPTIN*$^{-/-}$ serum were significantly elevated,
188 indicating that fibrogenesis had occurred, although the levels of LN and CIV
189 demonstrated no differences between *LEPTIN*$^{-/-}$ and WT livers (Figure 3F). These
190 suggest that the severity of the fibrotic lesions in *LEPTIN*$^{-/-}$ livers was most likely in
191 the middle or advanced stage of fibrosis but not cirrhosis. The expression of fibrotic
192 markers, *TGFB*, *ACTA2*, *LRAT* and *COL1A1*, were increased greatly in *LEPTIN*$^{-/-}$
193 livers (Figure 3G). Previous studies had shown that *CTHRC1* limits collagen
194 deposition (13); *TIMP1* inhibits the degradation of the main components of the
195 extracellular matrix (14); and *SERPINE1* inhibits the dissolution of fibrinolysis (15).
196 The reduction of *CTHRC1* and elevation of *TIMP1* and *SERPINE1* expression helps
197 explain the observed collagen accumulation in *LEPTIN*$^{-/-}$ livers.
198

Following additional H&E staining, PAS staining, Sirius red staining, Brunt's scoring criteria and Scheuer scoring criteria (16), the stage of non-alcoholic liver inflammation and fibrosis in *LEPTIN*$^{-/-}$ pigs was determined. The statistical results showed that the average NASH score was 4.47±0.86 at 12-22 months in *LEPTIN*$^{-/-}$ pig. By 22-35 months, the average fibrosis score in *LEPTIN*$^{-/-}$ pig was 3.00±0.27. In humans, the highest score observed clinically is 4.0. Thus, the stage of fibrosis in *LEPTIN*$^{-/-}$ pigs was clinically assessed in the range of moderate and severe (Table 1).

Porcine LEPTIN deficiency results in lipid peroxidation via the JAK2-STAT3 pathway

To identify the mechanism driving liver fibrosis in *LEPTIN*$^{-/-}$ pigs, several signaling pathways proven to be affected by LEPTIN were analyzed. Utilizing WB and real-time PCR analyses, no significant changes in the expression of mTOR, MAPK and PI3K-AKT pathway related proteins and genes were observed (Figure 4- figure supplement 1). Interestingly, phosphorylation of JAK2 and STAT3 was significantly reduced in *LEPTIN*$^{-/-}$ livers. In addition, altered expression of genes and proteins related to the JAK-STAT signaling pathway was also observed in response to LEPTIN deletion (Figure 4A & Figure 4- figure supplement 1B). The WB assay demonstrated that the phosphorylation of JAK2 and STAT3 was significantly reduced in *LEPTIN*$^{-/-}$ cells (Figure 4A). In particular, SOCS3, a negative regulator of cytokines and hormone transduction (17), and SREBP-1c, related to fat synthesis (18) were analyzed. STAT directly inhibits SREBP-1c, and SOCS3 promotes SREBP-1c

expression (19). Both SOCS3 and SREBP-1c expression was elevated in *LEPTIN*$^{-/-}$ livers (Figure 4B). Up-regulation of ACSL3 and ACSL5 in *LEPTIN*$^{-/-}$ indicates increased synthesis of acyl-CoA. The expression of CPT1a and CPT2 were also up-regulated in *LEPTIN*$^{-/-}$ livers, suggesting that FFA oxidation was activated. Immunofluorescence staining of SOCS3, SREBP1c and ACSL3 demonstrated increased expression in *LEPTIN*$^{-/-}$ fibrotic livers, suggesting that FFA synthesis was enhanced. In addition, the increased CPT1a and CPT2 expression suggested that acyl-coA transportation from the endoplasmic reticulum to mitochondria was enhanced (Figure 4- figure supplement 2).

Since LEPTIN deficiency affects β-oxidation, genes involved in the oxidation process were analyzed: *ACAT1* and *ACAT2* are acyl-coA transferases; *ACADM, ACADS* and *ACADL* are acyl-coA dehydrogenases; *ACSL1, ACSL3* and *ACSL5* are acyl-coA synthetizes; *ACOT7, ACOT8* and *ACOT12* are acyl-coA thioesterases; *Cpt1a, Cpt1b, Cpt1c* and *Cpt2* are carnitine transferases. Among them, *ACAT2*, *ACSL1*, *ACSL3*, *ACSL5*, *ACOT7*, *CPT1A*, *CPT1B* and *CPT2* were significantly up-regulated. This suggested that β-oxidation has mainly been strengthened during acyl-coA synthesis and transfer to the mitochondria (Figure 4C).

LEPTIN deficiency enhances gluconeogenesis and mitochondrial autophagy through the AMPK pathway in pigs

Gluconeogenesis disorder is the most typical feature of insulin resistance in which

HNF-4α synergizes with PGC-1α, FOXO1 and other key enzymes to induce gluconeogenesis (20), and Leptin regulates the AMPK pathway by inhibiting HNF-4α and promoting SIRT1 expression (21). In addition, PEPCK and G6Pase are speed limiting enzymes of glycogenesis (22). Based on the conclusions of these previous studies, protein or gene expression levels of these markers in biological pathways or biochemical processes in *LEPTIN*$^{-/-}$ pig livers were detected. It confirmed that the lack of Leptin down-regulated phosphorylation of AMPK due to increased Hnf-4α and decreased SIRT1 expression in *LEPTIN*$^{-/-}$ pig livers. PEPCK and G6Pase were also significantly up-regulated (Figure 4D&E). In addition, the fluorescence staining results demonstrate increased PEPCK and G6Pase expression with highly expressed α-SMA in *LEPTIN*$^{-/-}$ fibrotic livers, especially in the portal and perivenous areas (Figure 4- figure supplement 3).

SIRT1 regulates mitochondrial autophagy and proliferation through PINK1/Parkin and PGC-1α/TFAM, respectively (23). Initially markers of mitochondrial autophagy, Beclin1, LC3-II and P62 (24) were examined. The expression levels of PINK1 and phosphorylation of PARKIN were largely increased (Figure 4F), and the expression of Beclin1, LC3-II and P62 were also significantly increased in *LEPTIN*$^{-/-}$ livers (Figure 4G**)**. In contrast with the autophagy related genes, most of the mitochondrial synthesis related genes were not altered in *LEPTIN*$^{-/-}$. No expression changes for the mtDNA genes *ATP6, COX1* and *ND1* were observed via qPCR (Figure 4- figure supplement 4A). mtDNA copy number was calculated using Gcg as the internal

reference, and the mtDNA copy number was not altered in *LEPTIN*$^{-/-}$ pig livers (Figure 4- figure supplement 4B), suggesting that the down-regulation of SIRT1 in *LEPTIN*$^{-/-}$ pig livers enhances mitochondrial autophagy but does not affect mitochondrial synthesis.

LEPTIN$^{-/-}$ pigs undergo oxidative stress

Both lipid peroxidation and mitochondrial autophagy produce excessive ROS which in turn causes oxidative stress (25). Heatmap analysis based on DEGs and expression difference fold change was performed using the Omicshare software (Figure 5- figure supplement 1). GO enrichment analysis identified oxidation-reduction GO terms enriched for DEGs (Figure 5- figure supplement 2). In addition, the CYP2 mediated arachidonic acid metabolism and exogenous toxic substances metabolic pathways were unexpectedly enriched for DEGs in *LEPTIN*$^{-/-}$ pig livers (Figure 5- figure supplement 3 & Table. S2). Since the CYP2 enzyme mediates oxidative stress (26), real-time PCR was utilized to monitor the expression of CYP2 family genes (Figure 5A). The level of CYP2E1 in *LEPTIN*$^{-/-}$ liver was nearly 3 times higher than in WT (Figure 5B). The SOD enzyme activity was significantly reduced in *LEPTIN*$^{-/-}$ livers and sera, which could contribute to the excessive accumulation of ROS. Meanwhile, NO was up-regulated, and its reaction with OH increased the production of toxic ROS, which in turn led to increased MDA (Figure 5C-E). These data indicate that LEPTIN deletion enhances oxidative stress in pig livers.

LEPTIN deficient rat livers are void of hepatic fibrosis, mitochondrial autophagy and oxidative stress

Interestingly, published studies and data presented in this study demonstrate that, in contrast with pigs, Leptin deficiency in rodents does not result in hepatic fibrosis (27, 28). Compared with WT rats, the *Leptin*$^{-/-}$ rats have larger body and liver sizes (Figure 6A). H&E staining of *Leptin*$^{-/-}$ rat livers revealed fatty liver, lipid degeneration and balloon-like degeneration (Figure 6B). Sirius red staining, α-SMA staining and the four serum hepatic fiber indicators analysis showed no obvious collagen accumulation and fibrogensis occurring in *Leptin*$^{-/-}$ rat livers (Figure 6B-C). Furthermore, testing for SOD, MDA and NO found no obvious differences between *Leptin*$^{-/-}$ and WT rat livers (Figure 6- figure supplement 1A-C). This suggests that oxidative stress does not occur in *Leptin*$^{-/-}$ rat livers. WB and immunofluorescence staining revealed that the level of CYP2E1 was lowered (Figure 6D & Figure 6- figure supplement 1D). To investigate whether Leptin deletion in rats alters the JAK2-STAT3 pathway, p-JAK2/JAK2, p-STAT3/STAT3, SREBP-1C, SOCS3, CPT-1A and CPT-2 expressions were analyzed by WB and immuno-fluorescence staining. As observed in the *LEPTIN*$^{-/-}$ pig liver, the level of p-JAK2 and p-STAT3 were decreased compared to WT rat livers (Figure 6- figure supplement 2A) whereas the SREBP-1C and SOCS3 were significantly increased in *Leptin*$^{-/-}$ rat livers (Figure 6- figure supplement 2B&C), suggesting that the FFA synthesis was activated in *Leptin*$^{-/-}$ rat liver. However the expression of CPT-1A and CPT-2 in *Leptin*$^{-/-}$ rat livers were not altered (Figure 6-figure supplement 2B&C).

Previous studies in pigs have demonstrated that Leptin deficiency promotes mitochondrial autophagy, representing another major source of oxidative stress. Therefore, mitochondrial autophagy related markers were examined. Beclin1, LC3-Ⅱ and P62 expression showed no significant differences between *Leptin*$^{-/-}$ and control rats (Figure 6- figure supplement 3A). It was interesting to note that, in contrast with *LEPTIN*$^{-/-}$ pigs, SIRT1 expression in *Leptin*$^{-/-}$ rat liver was up-regulated (Figure 6-figure supplement 3B). This is quite different from the results in pigs and may be a key reason why *Leptin*$^{-/-}$ rat livers do not have mitochondrial autophagy.

In order to investigate the underlying causes of this phenomenon of opposite trends in protein expression between the two animals, WB was performed to detect the phosphorylation of AMPK pathway related genes. Interestingly, in contrast with *LEPTIN*$^{-/-}$ pig, the phosphorylation of AMPK was significantly increased in *Leptin*$^{-/-}$ rats (Figure 6- figure supplement 3C), providing a mechanism through which SIRT1 expression declined as SOCS3 and SREBP-1C expression increased.

Discussion

The liver closely communicates with adipose tissue and liver injury is observed in nearly 80% of obese patients (29). Since mechanistic studies of liver fibrogenesis are difficult to conduct in patients, current knowledge of obesity-induced liver fibrosis is mainly derived from Leptin-deficient animal models. The choice of Leptin is based on

its important roles in mediating energy homeostasis. Serum Leptin concentrations demonstrate an association with NAFLD which is mediated through insulin secretory dysfunction and insulin resistance in obese patients (30). NAFLD, the hepatic manifestation of the metabolic syndrome, comprises steatosis, steatohepatitis, hepatic fibrosis, cirrhosis and hepatocellular carcinoma (31). However, both previously published studies and work presented here suggests that two of the most commonly used rodent models, *ob/ob* mouse and Zucker rat, do not develop fibrosis observed in NAFLD patients. In an effort to develop a model that displays fibrogenesis as observed by patients, a *LEPTIN*$^{-/-}$ pig model was created. Consistent with human clinical data, the *LEPTIN*$^{-/-}$ pigs demonstrated obstructed body glucose regulation leading to insulin resistance and type II diabetes by 12-months of age. Interestingly, around the same age (6-12 month), 60% of *LEPTIN*$^{-/-}$ pig livers displayed lipid deposition and hepatocyte steatosis. The severity of liver injury also worsened with age in *LEPTIN*$^{-/-}$ pigs. Lobular inflammation and hepatocyte ballooning appeared in 33% *LEPTIN*$^{-/-}$ of pig livers between 12-22 months, whereas 42.9% *LEPTIN*$^{-/-}$ pig livers developed various degrees of fibrosis by 22-35 months of age (Figure 2). The development of liver injury in *LEPTIN*$^{-/-}$ pigs mirrored the pathological progression of NAFLD observed in obese patients. *LEPTIN*$^{-/-}$ pigs appeared to closely model the process of fibrogenesis observed in patients, which supports their use for investigation of the mechanisms underlying fibrogenesis in patients.

The mechanisms leading to NAFLD are unclear to date. In obese subjects, FFAs seem

353 to be misrouted to ectopic sites like hepatic tissues, resulting in steatosis. Steatosis
354 induces the production of pro-inflammatory mediators like TNF-α, IL-6 and IL-1β.
355 These cytokines promote the recruitment and activation of Kupffer cells, which
356 induce inflammation and hepatic insulin resistance via SOCS3. The accumulation of
357 fat in the liver leads to lipotoxicity and dysfunctional mitochondria, which further
358 causes oxidative stress due to imbalanced ROS production and protective oxidants,
359 eventually leading to hepatocyte death in NAFLD patients. The reduced
360 phosphorylation of JAK2 and STAT3 in LEPTIN deficient pig livers led to hepatic
361 insulin resistance and increased fat synthesis marked by activation of SOCS3 and
362 SREBP-1c, respectively, further confirms the value of the pig model (Figure 4). This
363 data is consistent with observed alterations in the JAK/STAT pathways in the
364 pathogenesis of metabolic disease (32). The excess intracellular FFAs observed in
365 *LEPTIN*$^{-/-}$ pigs resulted in intrinsic endoplasmic reticulum stress. The toxic pathways
366 were represented through the generation of ROS and increased mitochondrial
367 β-oxidation, which further caused hepatocyte death and fibrosis. Interestingly, in
368 contrast with pigs, although the Leptin deletion in rats altered the JAK2 and STAT3
369 phosphorylation and caused fatty liver, the level of damage was not severe enough to
370 drive mitochondrial β-oxidation and oxidative stress, which may explain why fibrosis
371 did not occur in *Leptin*$^{-/-}$ rat livers (Figure 6).
372
373 The progression of NAFLD to NASH has been characterized as a mitochondrial
374 disease occurring at an early human disease stage (33). Lipotoxicity encompasses the

375 dysregulation of the intracellular lipid composition, resulting in mitochondria
376 dysfunction, stimulating ROS production, oxidative stress, and impaired FFA
377 oxidation (34, 35). AMPK is a heterotrimeric enzyme which regulates cell growth,
378 proliferation, autophagy and apoptosis (36). In NAFLD, activation of AMPK in the
379 liver inhibits the synthesis and oxidation of FFAs, leading to the reduction of ectopic
380 lipid accumulation and improved insulin action (37). The current study on *Leptin*$^{-/-}$
381 rats provided evidence that AMPK activation might be crucial for prevention of liver
382 damage. This is further supported by the observed inactivation of the AMPK pathway
383 in *LEPTIN*$^{-/-}$ pigs, which drove mitochondrial autophagy, hepatic cell death and
384 fibrosis. Whether LEPTIN is required for activation of the AMPK pathway, or AMPK
385 mediated autophagy appears as a defensive reaction to liver injury has not been
386 previously addressed in the pig. Nevertheless, one collective conclusion from our
387 study is that the activity of AMPK represents a potential predictive biomarker of the
388 severity of liver injury. Activation of AMPK using pharmacological agents may also
389 represent a potential therapeutic avenue for preventing the progress of NASH to
390 fibrosis.
391
392 Liver fibrosis is defined by the excessive accumulation of extracellular matrix (ECM)
393 proteins. Activated hepatic stellate cells (HSCs) in the liver are the major source of
394 collagen production, leading to an imbalance in the formation and degradation of the
395 ECM. Activation of HSCs in the injured liver is regulated by fibrogenic and
396 pro-inflammatory cytokines (38). Recent evidence demonstrated that adiponectin

induces apoptosis and inhibits activation of HSCs through the AMPK pathway (39). Thus, the reduced AMPK signaling observed in *LEPTIN*$^{-/-}$ pig livers may promote the activation of HSCs, which in turn induce the deposition of ECM proteins and development of fibrosis; whereas the activated AMPK in *Leptin*$^{-/-}$ rat livers may lead to the apoptosis of HSCs, preventing the accumulation of ECM proteins.

The underlying mechanisms by which NASH transitions to fibrosis are not completely understood. Hepatic fibrosis occurs in 40-50% of patients with NASH and approximately 30-40% of NAFLD patients develop NASH. It has been estimated that the hepatic fibrosis stage is the strongest predictor of mortality in NAFLD patients. The present understanding of the dynamics in NAFLD progression has emerged from genetically modified rodents, such as *ob/ob* mice and Zucker rats. These animals are universally used in obesity and diabetic research. However, they fail to develop hepatic fibrosis. The LEPTIN deficient pigs generated in this study mirror the progression of hepatic fibrosis observed in NAFLD patients. Loss of LEPTIN in pigs led to β-oxidation and oxidative stress and, in combination with AMPK mediated mitochondrial autophagy, increased liver fibrosis (Figure 7). In sum, LEPTIN-deficient pigs provide an ideal model to investigate the full spectrum of human NAFLD and develop new strategies for the diagnosis and treatment of NAFLD.

Materials and Methods

Animal experiments were approved by the Animal Care Committee of the China Agricultural University (Plan book number SKLAB-2016-84) and performed according to the Chinese Animal Welfare Act. All chemicals used were purchased from Sigma-Aldrich Co. (Alcobendas, Madrid, Spain) unless otherwise indicated.

Experimental animals

The pig species used to generate *LEPTIN*$^{-/-}$ pigs was the Chinese experimental mini-pig (10). Both wild type and *LEPTIN*$^{-/-}$ pigs were provided with same manufactured diet. The cereal grain in dry form has been ground to supply to the pigs using an ad libitum feeding at fixed time (7:00-8:00, 1.75kg max; 12:00-13:00, 1.25kg max; and 17:00-18:00, 1kg max) every day. As shown in Supplemental Table 5, the nutrition content of pig diets were changed with age. The *Leptin*$^{-/-}$ *r*ats were generated by the Sen Wu laboratory (11). Both wild type and *Leptin*$^{-/-}$ rats were provided with the same always abundant manufactured diet (Table S5).

Generation of *LEPTIN*$^{-/-}$ pigs

Zinc finger nuclease (ZFN) plasmids targeting the *LEPTIN* gene were designed by Sigma-Aldrich. Fetal fibroblasts were isolated from 30-day old male pig embryo. Approximately 1×10^6 CEMP fetal fibroblasts were transfected with 2μg of each ZFN vector. Following G418 selection (500μg/mL, Promega), positive clones were collected for somatic cell nuclear transfer. PCR was performed following by Sanger sequencing to confirm the genetic sequence of the *LEPTIN* target region (primer

441 sequence : Forward 5'-GATTGTGTGGAAGGGGAAGA-3', Reverse
442 5'-GAGGTCCGCACAGGCTCTC T-3'.

443

444 **Western blotting (WB)**

445 Total protein of adipose tissue, liver tissue, hypothalamus tissue and serum were
446 obtained from the mutant and wild-type pigs. Electrophoretically separated proteins
447 were detected by specific primary antibodies (Table S3).

448

449 **Enzyme linked immunosorbent assay (ELISA)**

450 Serum was isolated from blood collected from pigs after fasting overnight. ELISA kit
451 was used to detect porcine IL-1β, IL-6 and TNF-α (Dan Shi Biological Technology,
452 Shanghai).

453

454 **Growth parameters and body composition**

455 Body weight of *LEPTIN*$^{-/-}$ and control pigs were examined weekly or monthly. The
456 percentage of total body fat was determined by using multi-slice computed
457 tomography (MSCT) with 64 rows, 128-slice MSCT scanner (Siemens). MSCT was
458 performed with the following parameters: 120kV, 500ms, and 1.5mm splice thickness.
459 The 3D reconstruction and analysis of data were performed by Sygo Fastview
460 software.

461

462 **Assessment of clinical indicators of liver disease**

Triglycerides, insulin, cholesterol, HDL, LDL, AST, ALT, ALP and four indexes of hepatic fibrosis were analyzed by the Beijing CIC Clinical Laboratory, China Agricultural University Veterinary Teaching Hospital and the endocrinology department of Beijing Tongren Hospital.

HOMA model assessing type II diabetes

Homeostatic model assessment (HOMA) included the following values, calculated on the basis of two parameters of fasting plasma glucose and insulin: HOMA-IR=(FPG, mmol/L)×(FINS, mIU/L)/22.5, assessment of insulin resistance; HOMA-IS=1/(FPG, mmol/L)×(FINS, mIU/L), assessment of insulin sensitivity; HOMA-β=20×(FPG, mmol/L)/[(FPG, mmol/L)-3.5] (%), assessment of islet β cell function. FPG, Fasting plasma glucose and FINS, fasting insulin.

Intravenous glucose tolerance test (IVGTT)

After 12-15 hours of fasting, pig blood samples were collected from the anterior chamber vein. 50% glucose solution was injected into the ear vein with a dose of 1.2mL/kg. Glucose concentrations were measured at 0 min (before injection), 1 min, 5 min, 10 min, 15 min, 30 min, 60 min and 90 min (after injection).

Histological analysis

Adipose, liver and pancreatic tissues were fixed in 10% neutral buffered formalin solution and paraffin-embedded. 5μm-thick sections were used for hematoxylin-eosin

(H&E) analysis, oil red O dye detection, periodic acid schiff (PAS) analysis (Beijing Solarbio life science), and Sirius red (Beijing Solarbio life science) analysis. α-SMA (ab5694, abcam) antibody was used for immunofluorescence using the ABC method (Vector Laboratories).

RNA isolation and quantitative RT-PCR

Total RNA was isolated from pig fat or liver tissues by TRIzol and RNeasy Mini Kit (QIAGEN). Then RNA samples were reverse transcribed to cDNA by M-MLV reverse transcription kit (Promega). The levels of relevant mRNAs were quantitated by real-time PCR using One Step SYBR GREEN RT-PCR Kit (Roche) in a Light Cycler instrument (Roche Applied Science, Mannheim, Germany). The specific primers for related genes were designed by Primer3 (v.0.4.0), PrimerBank, primer premier5.0 and NCBI BLAST (Table S4).

Detection of oxidative stress markers

Blood samples were collected from pigs after fasting overnight. Liver tissue was homogenized in cold 0.9% normal saline. The determination of NO requires the use of a specific homogenate. The total SOD activity detection kit (WST-8 method) (Beyotime, S-0101), lipid oxidation (MDA) assay kit (Beyotime, S-0131) and nitric oxide detection kit (Beyotime, S-0021) were utilized following the manufacturer's instructions.

Transcriptome analysis

The total liver RNA of three *LEPTIN*$^{-/-}$ and WT pigs from 22-35 month of age was extracted. The library construction and sequencing were performed with the steps of purifying mRNA, interrupting mRNA, synthesizing cDNA, selecting fragments, and PCR amplification. The qualified libraries were generated on Illumina Cbot for cluster generation, and then Illumina HiSeqTM2500 was used for transcriptome Sequencing. The purity, concentration and integrity of RNA samples were measured by Nano Drop, Qubit 2.0 and Agilent 2100 before sequencing. The cDNA library was constructed using the Illumina TruseqTM RNA kit（Illumina, USA）. The sequencing read length is PE125. Nearly 50GB per sample of raw data was obtained by sequencing, and 6-8GB clean data of each sample was obtained after removal of reads containing low sequencing quality with connectors and duplicates. After clean reads were obtained, HISAT was used for sequence alignment with the reference genome (Sus_scrofa. Sscrofa10.2.dna.chromosome) to obtain the information of the reference genes and the Mapped reads were obtained. By using the Cuffdiff component of Cufflinks software, the gene expression levels were quantified. Pearson's correlation co-efficient (r^2) was used as an indicator to evaluate the biological correlation of repetition. Then FPKM was used to determine the expression abundance of transcripts. The absolute value of Log2 Fold Change ≥ 1, and the corrected P value (FDR) < 0.05, was taken as the key index to screen the differential genes. GO and KEGG software were used for differential genes enrichment and signaling pathways screening. In GO and KEGG analysis, $P < 0.05$ was used as the selection criteria. DAVID and KOBAS software

529 were used for gene function analysis. The RNA-Seq data was deposited in Gene
530 Expression Omnibus (GEO) under the accession number GSE176023.
531
532 **Statistical analysis**
533 The experimental data are presented as the mean ± SD and were analysed by paired
534 Student's *t* test using SPSS15.0 software to compare the mutant and wild-type pigs. *P*
535 value <0.05 was considered significant.
536
537 **Data availability**
538 The datasets during and/or analysed during the current study available from the
539 corresponding author on reasonable request.
540
541 **Competing interest statement**
542 The authors declare that they have no conflicts of interest.
543
544 **Acknowledgments**
545 We are grateful for the gift of *Leptin*$^{-/-}$ rats by Dr. Sen Wu. We thank Dr. Zuoxiang
546 Liang for the technical support. This work is supported by National Natural Science
547 Foundation of China 31972566, National Genetically Modified Organisms Breeding
548 Major Projects of China 2016ZX08009003-006, National Basic Research Program
549 2016YFA0100202.
550

551 *Author contributions:* T.T., Z.S., R.W., S.J., and Q.W. performed the experiments;
552 X.H., and N.L. analyzed the data; Y.X. conceived and designed the experiments, and
553 wrote the manuscript with input from all authors. All authors have read and approved
554 the manuscript.

555

556 **List of abbreviations:**

557 ACADL: acyl-CoA dehydrogenase long chain

558 ACADM: acyl-CoA dehydrogenase medium chain

559 ACADS: acyl-CoA dehydrogenase short chain

560 ACAT1/2: acetyl-CoA acetyltransferase 1/2

561 ACOT7/8/12: acyl-CoA thioesterase 7/8/12

562 ACSL1/3/5: Acyl-CoA synthetases 1/3/5

563 ACTA2: Alpha-actin 2

564 ALP: alkaline phosphatase

565 ALT: alanine aminotransferase

566 AMPK: AMP-activated protein kinase

567 AST: aspartate aminotransferase

568 ATP6: mitochondrial ATPase subunit 6

569 CEMP: Chinese miniature experiment pig

570 CIC: China isotope corporation

571 CIV: collagen type IV

572 COL1A1: collagen Type I Alpha 1

573 COX1: mitochondrial Cytochrome c oxidase subunit I

574 CPT 1A/1B/2: carnitine palmitoyltransferase 1A/1B/2

575 CTHRC1: collagen triple helix repeat containing 1

576 DEGs: differentially expressed genes

577 ECM: extracellular matrix

578 ELISA: enzyme linked immunosorbent assay

579 ELOVL6: elongaseofverylongchainfattyacids 6

580 FABP1: fatty acid binding protein

581 FASN: fatty acid synthetase

582 FDR: false discovery rate

583 FFA: free fatty acid

584 FINS: fasting plasma insulin

585 FPG: fasting plasma glucose

586 G6Pase: glucose-6 phosphatase

587 GAPDH: glyceraldehyde-3-phosphate dehydrogenase

588 GO: gene ontology

589 H&E: hematoxylin-eosin

590 HA: hyaluronic acid

591 HDL: high density lipoprotein

592 HISAT: hierarchical indexing for spliced alignment of transcripts

593 HNF-4α: hepatocyte nuclear factor 4-alpha

594 HOMAs: Homeostasis model assessment

595 HSCs: hepatic stellate cells

596 IL-1β/6: interleukin 1 beta/6

597 IR: insulin resistance

598 IS: insulin sensitivity

599 IVGTT: intravenous glucose tolerance test

600 JAK2: janus kinase 2

601 KEGG: kyoto encyclopedia of genes and genomes

602 LC3: microtubule associated protein 1 light chain 3

603 LDL: low density lipoprotein

604 LN: laminin

605 LRAT: lecithin retinol acyltransferase

606 MCP-1: monocyte chemotactic protein 1

607 MDA: malondialdehyde

608 MSCT: multi-slice computed tomography

609 NAFLD: non-alcoholic fatty liver disease

610 NASH: non-alcoholic steatohepatitis

611 ND1: mitochondrial NADH-ubiquinone oxidoreductase chain 1

612 NFKB: nuclear factor kappa-light-chain-enhancer of activated Bcells

613 NO: nitric oxide

614 PAS: periodic acid schiff

615 PEPCK: phosphoenolpyruvate carboxylase

616 PGC-1α: peroxisome proliferator activated receptor gamma coactivator 1 alpha

617 PIIINP: procollagen-III-peptide

618 PINK1: phosphatase and tensin homolog induced kinase 1

619 PPARA: peroxisome proliferator-activated receptor alpha

620 ROS: reactive oxygen species

621 SCD1: stearoyl-CoA desaturase 1

622 SERPINE1: serpin family E member 1

623 SIRT1: sirtuin 1

624 SOCS-3: suppressor of cytokine signaling-3

625 SOD: superoxide dismutase

626 SREBP-1c: sterol-regulatory element-binding protein-1c

627 STAT3: signal transducer and activator of transcription 3

628 TFAM: transcription factor A, mitochondrial

629 TGFB: transforming growth factor-beta

630 TIMP1: tissue inhibitor of matrix metalloprotease-1

631 TNF-α: tumor necrosis factor alpha

632 WB: western blotting

633 WT: wild type

634 ZFN: zinc finger nuclease technology

635 α-SMA: alpha smooth muscle actin

636

637 **References**

638 1. Brunt EM. Nonalcoholic steatohepatitis. Semin Liver Dis. 2004; 24(1):3-20.

2. Hebbard L, George J. Animal models of nonalcoholic fatty liver disease. Nat Rev Gastroenterol Hepatol. 2011; 8(1):35-44.

3. Asrani SK. Liver transplantation for nonalcoholic steatohepatitis. Clin Gastroenterol Hepatol. 2014; 12(3):403-4.

4. Browning JD, Horton JD. Molecular mediators of hepatic steatosis and liver injury. J Clin Invest 2004; 114(2): 147-152.

5. Weisberg SP, McCann D, Desai M, Rosenbaum M, Leibel RL, Ferrante AW. Obesity is associated with macrophage accumulation in adipose tissue. J Clin Invest 2003; 112(12): 1796-1808.

6. Romboms K, Marraf F. Molecular mechanisms of hepatic fibrosis in Non-alcoholic steatohepatitis. Dig Dis 2010; 28(1):229-1235.

7. Farooqi IS, O'Rahilly S. Leptin: a pivotal regulator of human energy homeostasis. Am J Clin Nutr 2009; 89(3): 980S-984S.

8. Leclercq IA, Farrell GC, Schriemer R, Robertson GR. Leptin is essential for the hepatic fibrogenic response to chronic liver injury. J Hepatol 2002; 37(2): 206-213.

9. Ikejima K, Takei Y, Honda H, Hirose M, Yoshikawa M, Zhang YJ, et al. Leptin receptor-mediated signaling regulates hepatic fibrogenesis and remodeling of extracellular matrix in the rat. Gastroenterology 2002; 122(5): 1399-1410.

10. Fan B, Yang SL, Liu B, Yu M, Zhao SH, Li K. Characterization of the genetic diversity on natural populations of Chinese miniature pig breeds. Anim Genet 2003; 34(6):465-6.

11. Lan H, Li S, Guo Z, Men H, Wu Y, Li N, et al. Efficient generation of selection-gene-free rat knockout models by homologous recombination in ES cells. FEBS Lett 2016; 590(19):

3416-3424.

12. Machado M, Marques-Vidal P, Cortez-Pinto H. Hepatic histology in obese patients undergoing bariatric surgery. J Hepatol 2006; 45(4): 600-606.

13. LeClair R, Lindner V. The role of collagen triple helix repeat containing 1 in injured arteries, collagen expression, and transforming growth factor beta signaling. Trends Cardiovasc Med 2007; 17:202-205.

14. Giannandrea M, Parks WC. Diverse functions of matrix metalloproteinases during fibrosis. Dis Model Mech 2014; 7(2): 193-203.

15. Ghosh AK, Vaughan DE. PAI-1 in tissue fibrosis. J Cell Physiol 2012; 227:493-507.

16. Farrell GC, Chitturi S, Lau GK, Sollano JD. Asia-Pacific Working Party on NAFLD. Guidelines for the assessment and management of non-alcoholic fatty liver disease in the Asia-Pacific region: executive summary. J Gastroenterol Hepatol 2007; 22(6): 775-777.

17. Yumet G, Shumate ML, Bryant DP, Lang CH, Cooney RN. Hepatic growth hormone resistance during sepsis is associated with increased suppressors of cytokine signaling expression and impaired growth hormone signaling. Crit Care Med 2006; 34(5): 1420-1427.

18. Joseph SB, Laffitte BA, Patel PH, Watson MA, Matsukuma KE, Walczak R, et al. Direct and indirect mechanisms for regulation of fatty acid synthase gene expression by liver X receptors. J Biol Chem 2002; 277(13): 11019-11025.

19. Ueki K, Kondo T, Tseng Y H, Kahn CR. Central role of suppressors of cytokine signaling proteins in hepatic steatosis, insulin resistance, and the metabolic syndrome in the mouse. P Natl Acad Sci USA 2005; 102(38): 10422-7.

20. Mcglacken-Byrne SM, Hawkes CP, Flanagan SE, Ellard S, McDonnell CM, Murphy NP. The

683 evolving course of HNF4A hyperinsulinaemic hypoglycaemia-a case series. Diabetic Med
684 2014; 31(1): E1-E5.
685 21. Yu JW, Sun LJ, Liu W, Zhao YH, Kang P, Yan BZ. Hepatitis C virus core protein induces
686 hepatic metabolism disorders through down-regulation of the SIRT1-AMPK signaling pathway.
687 Int J Infect Dis 2013; 17:e539-545.
688 22. Goto M, Yoshioka T, Battelino T, Ravindranath T, Zeller WP. TNF alpha decreases
689 gluconeogenesis in hepatocytes isolated from 10-day-old rats. Pediatr Res 2001; 49(4):
690 552-557.
691 23. Sha D, Chin L S, Li L. Phosphorylation of parkin by Parkinson disease-linked kinase PINK1
692 activates parkin E3 ligase function and NF-kappaB signaling. Hum Mol Genet 2010; 19(2):
693 352-363.
694 24. Scarlatti F, Maffei R, Beau I, Codogno P, Ghidoni R. Role of non-canonical Beclin
695 1-independent autophagy in cell death induced by resveratrol in human breast cancer cells.
696 Cell Death Differ 2008; 15(8): 1318-1329.
697 25. Lee J, Ellis JM, Wolfgang MJ. Adipose fatty acid oxidation is required for thermogenesis and
698 potentiates oxidative stress-induced inflammation. Cell Rep 2015; 10(2): 266-279.
699 26. Leung TM, Nieto N. CYP2E1 and oxidant stress in alcoholic and non‐alcoholic fatty liver
700 disease. J Hepatol 2013; 58:395-398.
701 27. Leclercq IA, Farrell GC, Schriemer R, Robertson GR. Leptin is essential for the hepatic
702 fibrogenic response to chronic liver injury. J Hepatol 2002; 37(2): 206-213.
703 28. Ikejima K, Takei Y, Honda H, Hirose M, Yoshikawa M, Zhang YJ, et al. Leptin
704 receptor-mediated signaling regulates hepatic fibrogenesis and remodeling of extracellular

matrix in the rat. Gastroenterology 2002; 122(5): 1399-1410.

29. Williams CD, Stengel J, Asike MI, Torres DM, Shaw J, Contreras M, et al. Prevalence of Nonalcoholic Fatty Liver Disease and Nonalcoholic Steatohepatitis Among a Largely Middle-Aged Population Utilizing Ultrasound and Liver Biopsy: A Prospective Study. Gastroenterology 2011; 140(1): 124-131.

30. Hossain IA, Akter S, Rahman MK, Ali L. Gender specific Association of Serum Leptin and Insulinemic Indices with nonalcoholic fatty liver disease in Prediabetic subjects. PLoS One 2015; 10(11):e0142165.

31. Odenthal MT, Sminia ML, Prick LJ, Gortzak-Moorstein N, Völker-Dieben HJ. Long-term follow-up of the corneal endothelium after artisan lens implantation for unilateral traumatic and unilateral congenital cataract in children - Two case series. Cornea 2006; 25(10): 1173-1177.

32. Penas-Steinhardt A, Tellechea ML, Gomez-Rosso L, Brites F, Frechtel GD, Poskus E. Association of common variants in JAK2 gene with reduced risk of metabolic syndrome and related disorders. BMC Med Genet 2011; 12:166.

33. Pessayre D, Fromenty B. NASH: a mitochondrial disease. J. Hepatol 2005; 42(6): 928-940.

34. Vial G, Dubouchaud H, Couturier K, Cottet-Rousselle C, Taleux N, Athias A. Effects of a high-fat diet on energy metabolism and ROS production in rat liver. J Hepatol 2011; 54:348~356

35. Jeon SM. Regulation and function of AMPK in physiology and diseases. Exp Mol Med 2016; 48(7):e245

36. Smith BK, Marcinko K, Desjardins EM, Lally JS., Ford RJ., Steinberg GR. Treatment of

Nonalcoholic Fatty Liver Disease: Role of AMPK. Am J Physiol Endocrinol Metabol 2016; 311:E730-E740.

37. Bataller R, Brenner DA. Liver fibrosis. J Clin Invest 2005; 115:209–218.

38. Luedde T, Schwabe RF. NF-κB in the liver--linking injury, fibrosis and hepatocellular carcinoma. Nat Rev Gastroenterol Hepatol 2011; 8:108–118.

39. Byrne CD, Targher G. NAFLD: a multisystem disease. Hepatol 2015; 62(1):S47-S64.

Figure legends

Figure 1. Generation and phenotyping of *LEPTIN*$^{-/-}$ pigs.

A. Body sizes of *LEPTIN* mutant and WT pigs. Yellow scale bar represents 1meter. **B.** Monthly weight records of pigs. N=3/group. **C.** MSCT scan tomography showing body fat distribution in *LEPTIN* mutant and WT pigs. The red area and white arrows indicated adipose tissue. The scale bar represents 50 mm. **D.** Blood glucose, plasma triglyceride and plasma total cholesterol levels in *LEPTIN* mutant and WT pigs. **E.** Plasma insulin levels in *LEPTIN* mutant and WT pigs. **F.** HOMA-IR results evaluating insulin resistance for pigs at different ages. **G.** IVGTT assay to assess blood glucose regulation. N=3/group. The bars represent the mean±SD; *P<0.05, **P<0.01, and ***P<0.001; NS, non-significant.

Figure 1- figure supplemental 1. Generation of *LEPTIN* mutant pigs.

A. Porcine *LEPTIN* gene targeting scheme (targeting site in red). **B.** Construction of ZFN target vector. **C.** Positive clones and observed *LEPTIN* mutations. **D.** Sequence

749 analysis of *LEPTIN* mutants. Peak maps shown mutated base pairs in *LEPTIN* gene
750 on three different chromatids.

751

752 **Figure 1- figure supplemental 2. Detection of Leptin in mutant pigs.**

753 **A.** The level of Leptin in subcutaneous fat and visceral fat was measured by WB. **B.**
754 WB of Leptin expression in serum.

755

756 **Figure 1- figure supplemental 3. Analysis of obesity phenotypes in *LEPTIN*$^{-/-}$**
757 **pigs.**

758 **A.** Maximum thickness of subcutaneous fat and the percentage of body fat in
759 *LEPTIN*$^{-/-}$ and WT pigs. **B.** HE staining of adipose tissue. Bar=100μm. **C.** Serum high
760 density lipoprotein (HDL) and low density lipoprotein (LDL) concentrations. The
761 bars represent the mean ± SD; NS, non-significant.*P<0.05. Bar=20μm.

762

763 **Figure 1- figure supplemental 4. Analysis of the type II diabetes in *LEPTIN*$^{-/-}$**
764 **pigs.**

765 **A.** HOMA-IS analysis to evaluate insulin sensitivity and HOMA-β analysis to
766 evaluate function of β cells for pigs at different ages. **B.** H&E staining and insulin
767 immuno-fluorescence of pig pancreatic tissue. Dotted box and arrows indicate islet
768 and β cells (insulin positive). The bars represent the mean ± SD; NS,
769 non-significant.*P<0.05. Bar=20μm.

770

Figure 2. Progression of liver injury in *LEPTIN*$^{-/-}$ pigs.

H&E and stage-specific staining demonstrating histological alterations and injury of hepatocytes in *LEPTIN* mutant and WT pigs over time. Oil red O staining for lipid deposition (**A&B**), PAS staining for glycogen storage (**C**), and sirius red staining for collagen deposition (**D**). Scale bar represents 50μm.

Figure 3. Pathological and molecular detection of liver injury in *LEPTIN*$^{-/-}$ pigs.

Triglyceride concentrations **(A)** and expression of genes related to FFA synthesis **(B)** in *LEPTIN* mutant and WT pigs. Expression of inflammation related genes in liver **(C)** and the concentration of inflammatory cytokines, IL-1β, IL-6 and TNF-α in serum **(D)**. N=3-5/group. **E.** Gross images, H&E and immunofluorescent staining for α-SMA in 25-month-old *LEPTIN* mutant and WT livers (bar=20μm). **F.** Liver functional status and expression of liver fibrosis markers in serum. **G.** Expression of genes related to fibrogenesis. N=3-5/group. The bars represent the mean±SD; *P<0.05; NS, non-significant.

Figure 4. Alteration of JAK-STAT and AMPK pathway related genes in *LEPTIN*$^{-/-}$ pig livers.

A. WB analysis of JAK-STAT signaling proteins. **B.** WB analysis of FFA synthesis and oxidation related proteins. **C.** Expression of β-oxidation related genes. **D.** WB analysis of AMPK signaling proteins. **E.** Expression of gluconeogenesis related genes. **F.** WB analysis of SIRT1-mediated autophagy related proteins. **G.** WB analysis of

mitochondrial autophagy markers. N=3/group. The bars represent the mean±SD; *P<0.05.

Figure 4- figure supplemental 1. The effects of LEPTIN deficiency on mTOR, MAPK and PI3K-AKT pathways in pig livers.

A. WB analysis of mTOR, PI3K-AKT, MAPK pathway related proteins**. B.** Expression of mTOR, MAPK, and PI3K-AKT pathway related genes detected by qPCR. The bars represent the mean ± SD; *P<0.05.

Figure 4- figure supplemental 2. Histological detection of proteins affected by JAK-STAT signaling.

Immunofluorescence staining of JAK-STAT pathway related proteins involved in FFA synthesis and β-oxidation process. The white dashed box indicated the enlarged area. Bar=100μm.

Figure 4- figure supplemental 3. Histological detection of proteins affected by AMPK signaling.

Immunofluorescence staining of AMPK pathway related proteins involved in gluconeogenesis. The white dashed box indicated the enlarged area. Bar=100μm.

Figure 4- figure supplemental 4. Effects of *LEPTIN* knockout on mitochondrial function in pig livers.

A. Expression analysis of mitochondrial synthesis and autophagy related genes by qPCR. **B.** Measurement of Mitochondrial DNA copy numbers. The bars represent the mean ± SD; NS, non-significant.*P<0.05.

Figure 4- source data. Original files of western blot.

Figure 5. Detection of oxidative stress in *LEPTIN*$^{-/-}$ pig livers.

A. Expression analysis of CYP2 family genes by real-time PCR. **B.** WB analysis and Immunofluorescence staining of CYP2E1. Scale bar represents 100μm. **C-E.** Detection of oxidative stress markers in the liver and serum. Content of MDA **(C),** NO **(D)** and SOD **(E)**. N=3/group. The bars represent the mean±SD; *P<0.05.

Figure 5- figure supplemental 1. Heatmap of DEGs between *LEPTIN*$^{-/-}$ and WT pig livers.

Heatmap displaying the relative expression of DEGs in liver samples from three WT and *LEPTIN*$^{-/-}$ pigs assessed via RNA-seq. Red indicates up-regulated and blue indicates down-regulated genes.

Figure 5- figure supplemental 2. GO terms enriched for DEGs.

A. Enrichment of molecular function, biological process and cell component GO terms. The ordinate represents the entry names for different functions, processes and components, and the abscissa represents the number of genes enriched on that entry. **B.**

837 Molecular functional pattern of enriched GO terms. Each node represents a GO term,
838 and the darkness of the color indicates the degree of enrichment. The term name and
839 corrected *P*-value are shown for each node. The node terms **(a)** and **(b)** represent the
840 two most highly enriched of the molecular functions. **C.** Biological process pattern of
841 enriched GO terms. The node terms **a**, **b**, **c** and **d** are the four most highly enriched
842 biological processes.

843

844 **Figure 5- figure supplemental 3. P450 enzyme (CYP2) related KEGG pathways**
845 **enrichment for DEGs.**

846 Boxes represent molecular compounds, solid arrows represent chemical reactions, and
847 dotted arrows represent indirect reactions. Red boxes represent DEGs. **A.** Metabolism
848 of xenobiotics by cytochrome P450 (00980). **B.** Arachidonic acid metabolism
849 pathway (00590).

850

851 **Figure 5- source data. Original files of western blot.**

852

853 **Figure 6. Analysis of liver injury and related signaling pathways in *Leptin*$^{-/-}$ rats.**

854 **A.** Comparison of *Leptin*$^{-/-}$ and WT rat bodies and livers. **B.** H&E, Sirius red and
855 α-SMA staining analysis of rat livers. Scale bar represents 100μm. **C.** Detection of
856 fibrosis markers in serum.

857

858 **Figure 6- figure supplemental 1. Oxidative stress analysis in *Leptin*$^{-/-}$ rat liver.**

A-C. Analysis of oxidative stress markers, MDA **(A),** NO **(B) and** SOD **(C)**, in the *Leptin*$^{-/-}$ rat liver and serum. n=3. The bars represent the mean±SD; NS, non-significant. **D**. Immunofluorescence staining of CYP2E1. The white dashed box indicated the enlarged area. Bar=100μm.

Figure 6- figure supplemental 2. Analysis JAK-STAT pathway related signaling and histological detection of proteins affected by JAK-STAT pathway in *Leptin*$^{-/-}$ rats.

A. WB analysis of CYP2E1 in rat livers. **B.** WB analysis of JAK-STAT pathway related proteins in rat livers. Gray scale quantitative analysis of JAK2/p-JAK2 and STAT3/p-STAT3 protein expression. The bars represent the mean ± SD; *P<0.05. NS, non-significant. **C.** Immunofluorescence staining of JAK-STAT pathway related proteins involved in FFA synthesis and β-oxidation processes. The white dashed box indicated the enlarged area. Bar=100μm.

Figure 6- figure supplemental 3. Analysis AMPK pathway related signaling and histological detection of proteins affected by AMPK pathway in *Leptin*$^{-/-}$ rats.

A. WB analysis of mitochondrial autophagy related markers. **B.** Immunofluorescence staining of AMPK pathway related proteins involved in mitochondrial autophagy. The white dashed box indicated the enlarged area. Bar=100μm. **C.** WB analysis of AMPK and p-AMPK proteins. Gray scale quantitative analysis of AMPK/p-AMPK protein

880 expression. n=3/group. The bars represent the mean±SD; *P<0.05. NS,
881 non-significant.

882

883 **Figure 6- source data. Original files of western blot.**

884

885 **Figure 7. Proposed mechanistic model of fibrosis progression in *LEPTIN*$^{-/-}$ pig**
886 **liver.**

887 Reduction of p-AMPK promotes mitochondrial autophagy. Meanwhile, activation of
888 JAK2/STAT3 signaling pathway leads to enhanced FFA oxidation and oxidative stress.
889 Oxidative stress drives the development liver fibrosis in *LEPTIN*$^{-/-}$ pigs.

890

891 **Table 1. Assessment of liver fibrosis and NASH staging in pigs.**

892 Brunt's and Scheuer scoring criteria were used to determine the stage of non-alcoholic
893 liver inflammation and fibrosis in *LEPTIN*$^{-/-}$ and WT pigs.

894

895 **Supplemental Table 1. Analysis of off-target mutations in *LEPTIN*$^{-/-}$ pigs.**

896 Sequence locations were obtained by whole pig genome BLAST with ZFN cut site
897 sequences. The yellow part represents the target site section, with each homologous
898 section and the chromosome position on the genome listed below. “No” meant that
899 there was no genetic mutation detected.

900

901 **Supplemental Table 2. KEGG pathways were enriched for DEGs.**

902 The analysis of pathway enrichment was based on the KEGG pathway analysis ($P<$
903 0.05), and hypergeometric tests were used to screen the pathways with significant
904 enrichment.

905

906 **Supplemental Table 3. The list of antibodies used in this study.**

907 In this table, the item No. and manufacturer of all antibodies used in this study for
908 WB and immunofluorescence staining are listed in details.

909

910 **Supplemental Table 4. The list of primers used in this study.**

911 In this table, the sequence of all primers used in the study for quantitative PCR are
912 listed in details.

913

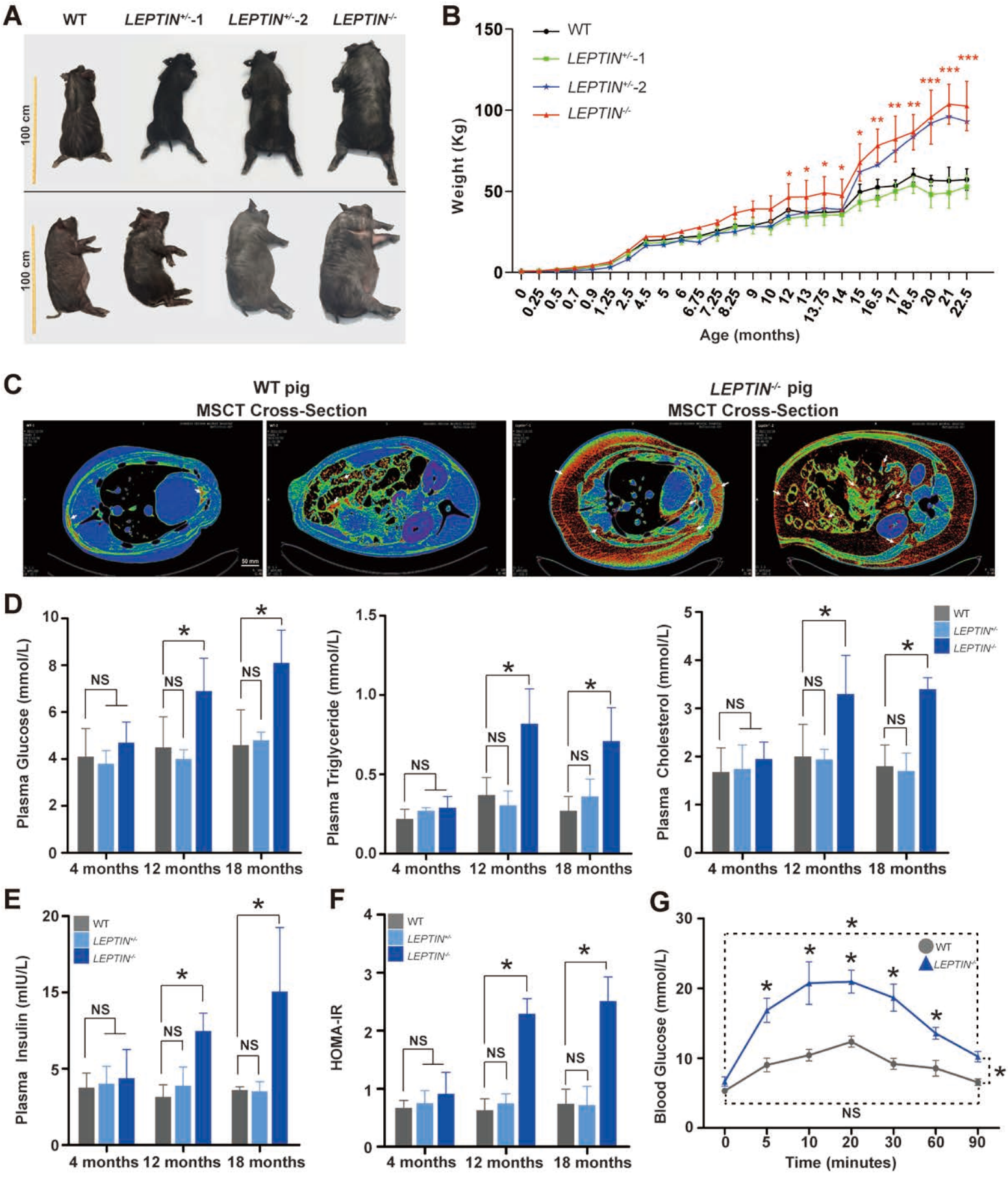
A
WT
LEPTIN+/--1
LEPTIN+/--2
LEPTIN-/-
100 cm
100 cm
B
WT
LEPTIN+/--1
LEPTIN+/--2
LEPTIN-/-
Weight (Kg)
Age (months)
C
WT pig
MSCT Cross-Section
LEPTIN-/- pig
MSCT Cross-Section
50 mm
D
Plasma Glucose (mmol/L)
Plasma Triglyceride (mmol/L)
Plasma Cholesterol (mmol/L)
NS
4 months
12 months
18 months
E
Plasma Insulin (mIU/L)
F
HOMA-IR
G
Blood Glucose (mmol/L)
Time (minutes)

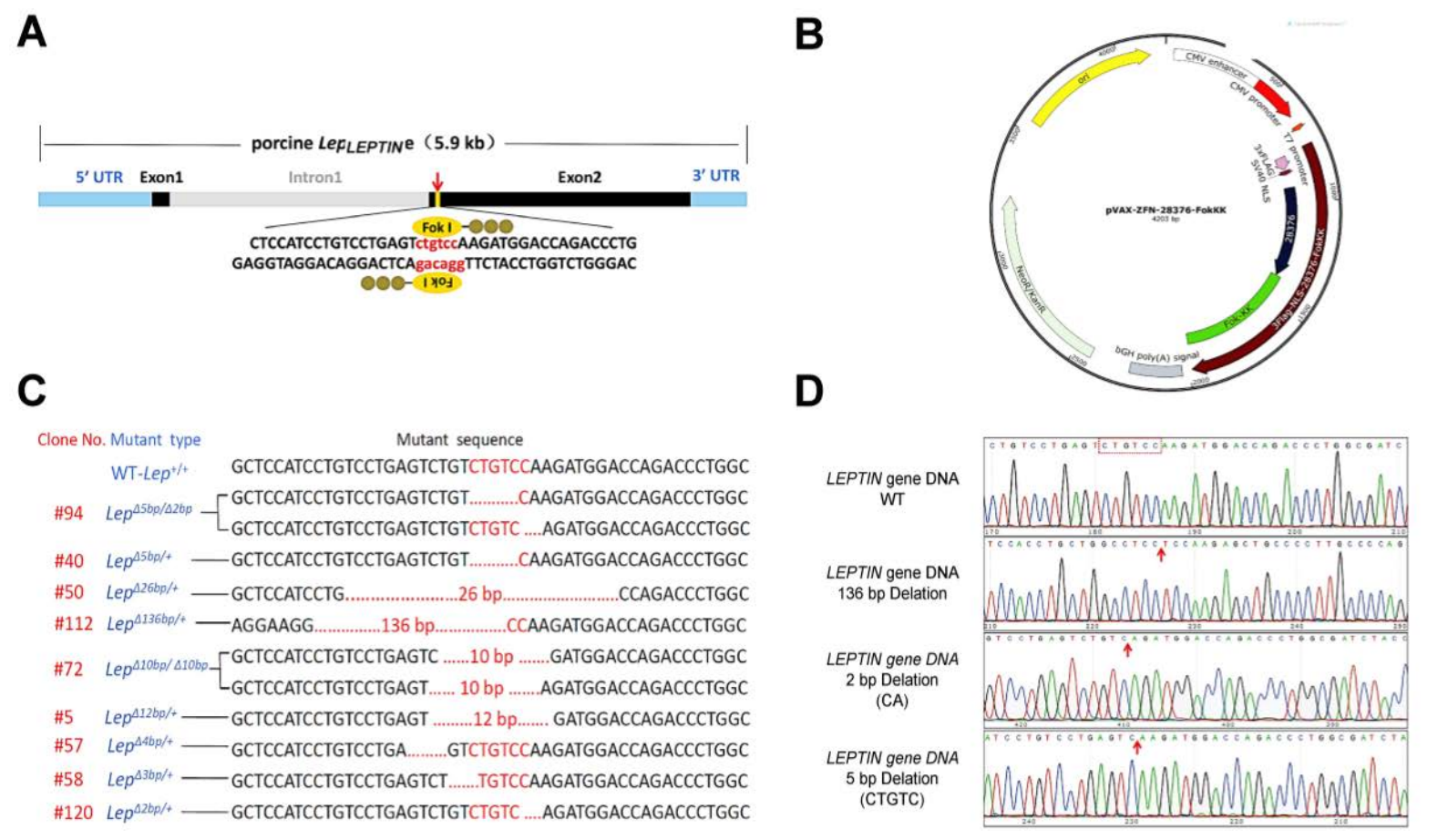
A
porcine Lep LEPTIN e (5.9 kb)
5′ UTR
Exon1
Intron1
Exon2
3′ UTR
Fok I
CTCCATCCTGTCCTGAGTctgtccAAGATGGACCAGACCCTG
GAGGTAGGACAGGACTCAgacaggTTCTACCTGGTCTGGGAC
Fok I
B
pVAX-ZFN-28376-FokKK
4203 bp
ori
CMV enhancer
CMV promoter
T7 promoter
3xFLAG
SV40 NLS
28376
Fok KK
bGH poly(A) signal
NeoR/KanR
C
Clone No.
Mutant type
Mutant sequence
WT-Lep+/+
GCTCCATCCTGTCCTGAGTCTGTCTGTCCAAGATGGACCAGACCCTGGC
#94
Lep Δ5bp/Δ2bp
GCTCCATCCTGTCCTGAGTCTGT.....CAAGATGGACCAGACCCTGGC
GCTCCATCCTGTCCTGAGTCTGTCTGTC ....AGATGGACCAGACCCTGGC
#40
Lep Δ5bp/+
GCTCCATCCTGTCCTGAGTCTGT.....CAAGATGGACCAGACCCTGGC
#50
Lep Δ26bp/+
GCTCCATCCTG.....26 bp.....CCAGACCCTGGC
#112
Lep Δ136bp/+
AGGAAGG.....136 bp.....CCAAGATGGACCAGACCCTGGC
#72
Lep Δ10bp/ Δ10bp
GCTCCATCCTGTCCTGAGTC .....10 bp .....GATGGACCAGACCCTGGC
GCTCCATCCTGTCCTGAGT..... 10 bp .....AGATGGACCAGACCCTGGC
#5
Lep Δ12bp/+
GCTCCATCCTGTCCTGAGT .....12 bp..... GATGGACCAGACCCTGGC
#57
Lep Δ4bp/+
GCTCCATCCTGTCCTGA.....GTCTGTCCAAGATGGACCAGACCCTGGC
#58
Lep Δ3bp/+
GCTCCATCCTGTCCTGAGTCT.....TGTCCAAGATGGACCAGACCCTGGC
#120
Lep Δ2bp/+
GCTCCATCCTGTCCTGAGTCTGTCTGTC ....AGATGGACCAGACCCTGGC
D
LEPTIN gene DNA
WT
LEPTIN gene DNA
136 bp Delation
LEPTIN gene DNA
2 bp Delation
(CA)
LEPTIN gene DNA
5 bp Delation
(CTGTC)

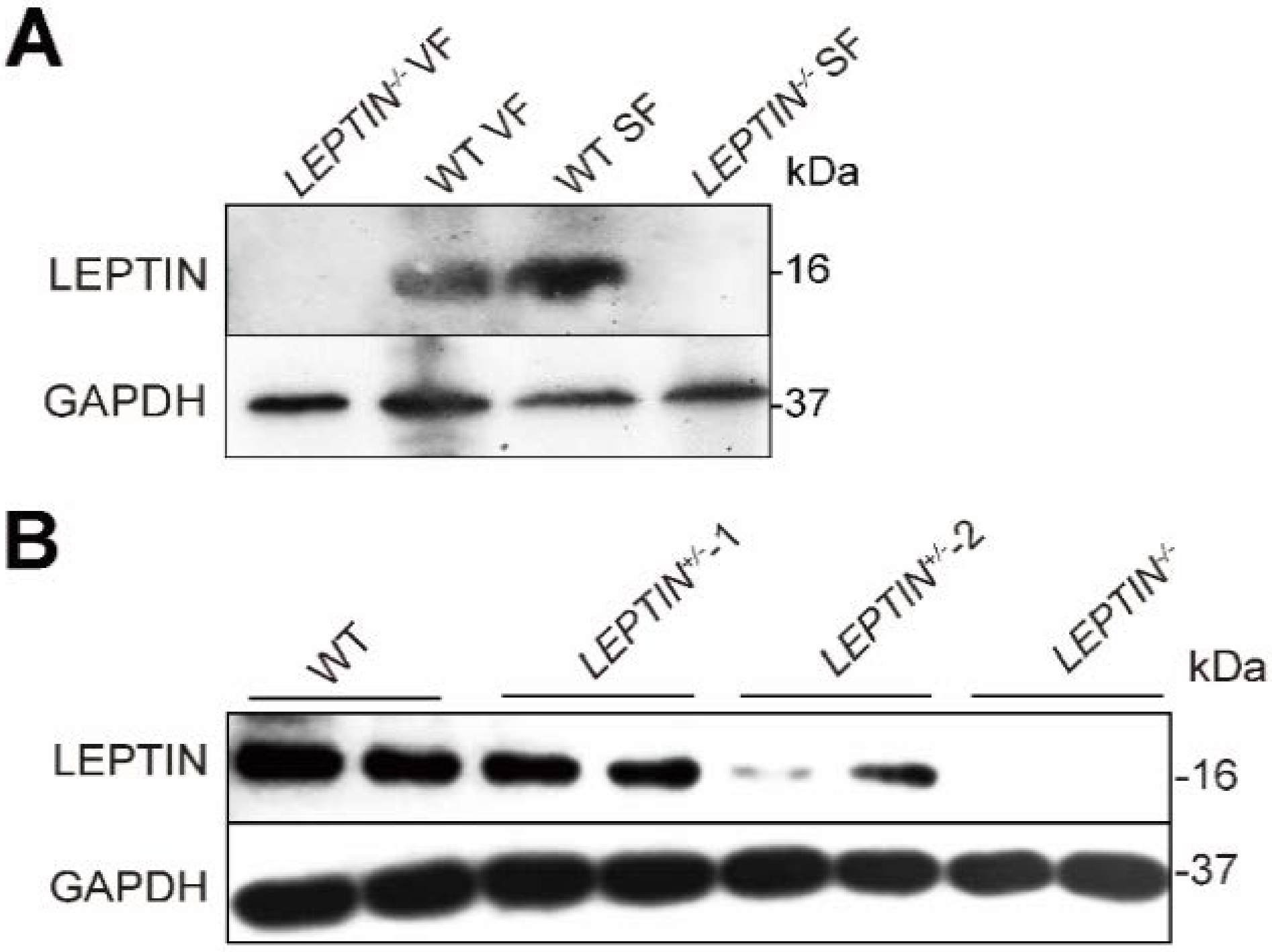
A
LEPTIN+/- VF
WT VF
WT SF
LEPTIN+/- SF
kDa
LEPTIN
16
GAPDH
37
B
WT
LEPTIN+/- 1
LEPTIN+/- 2
LEPTIN+/-
kDa
LEPTIN
16
GAPDH
37

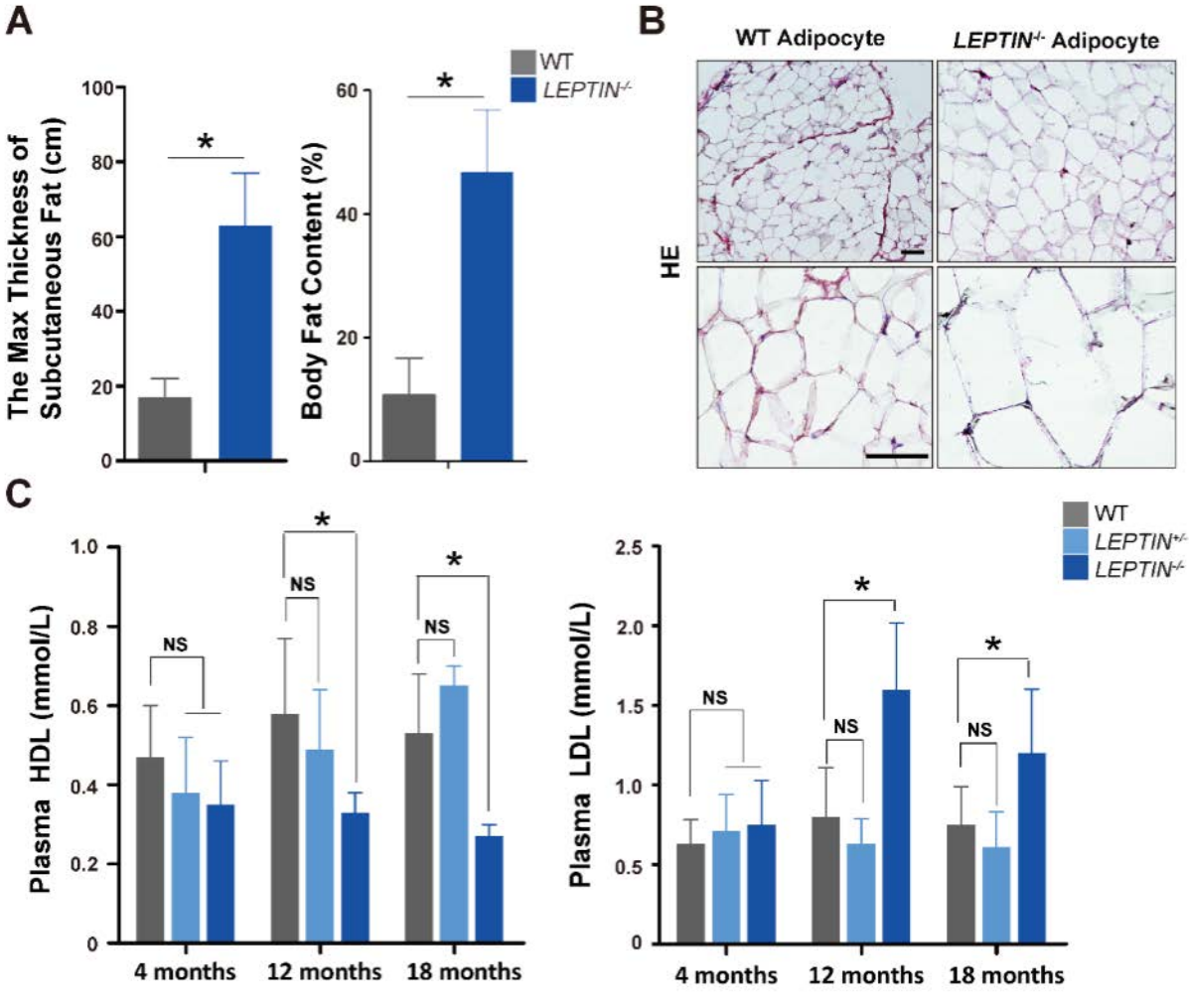
A
WT
LEPTIN-/-
The Max Thickness of Subcutaneous Fat (cm)
Body Fat Content (%)
*
B
WT Adipocyte
LEPTIN-/- Adipocyte
HE
C
WT
LEPTIN+/-
LEPTIN-/-
Plasma HDL (mmol/L)
Plasma LDL (mmol/L)
NS
4 months
12 months
18 months

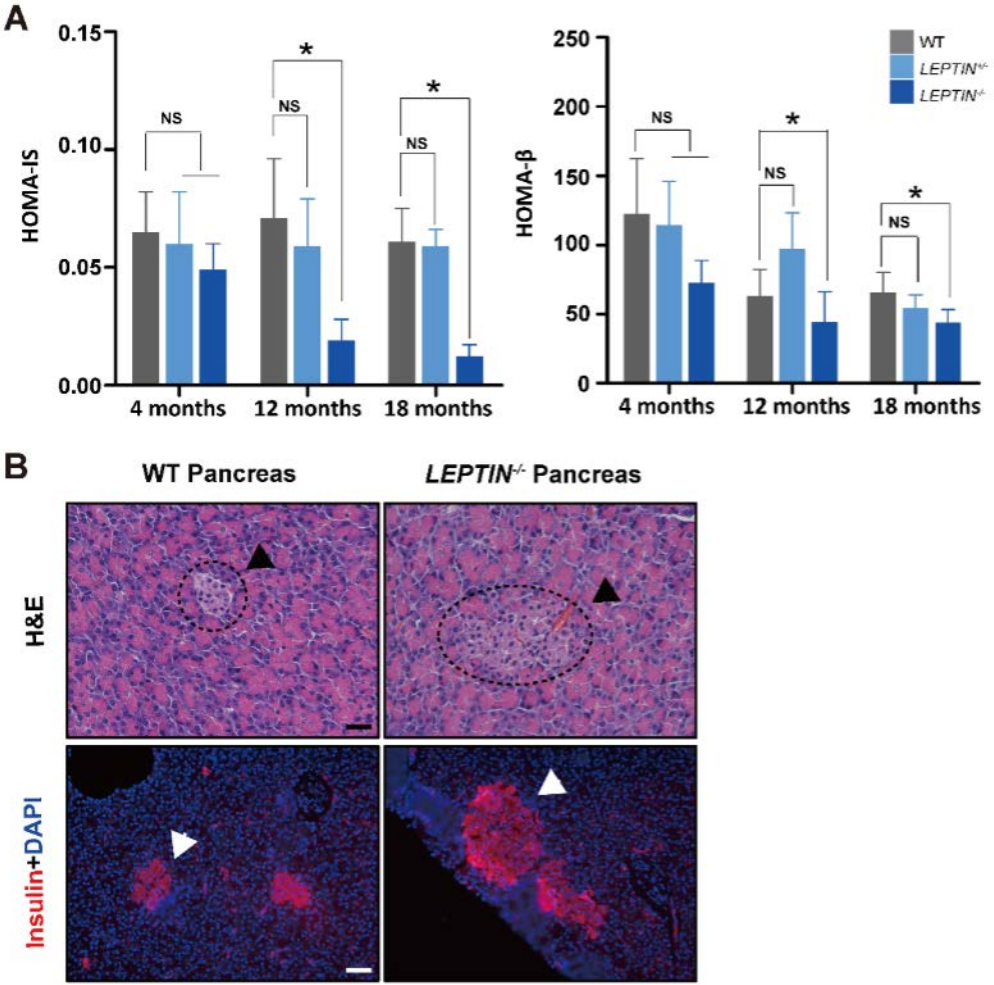
A
HOMA-IS
0.15
0.10
0.05
0.00
NS
NS
*
NS
*
4 months
12 months
18 months
HOMA-β
250
200
150
100
50
0
WT
LEPTIN+/-
LEPTIN-/-
NS
*
NS
*
NS
4 months
12 months
18 months
B
WT Pancreas
LEPTIN-/- Pancreas
H&E
Insulin+DAPI

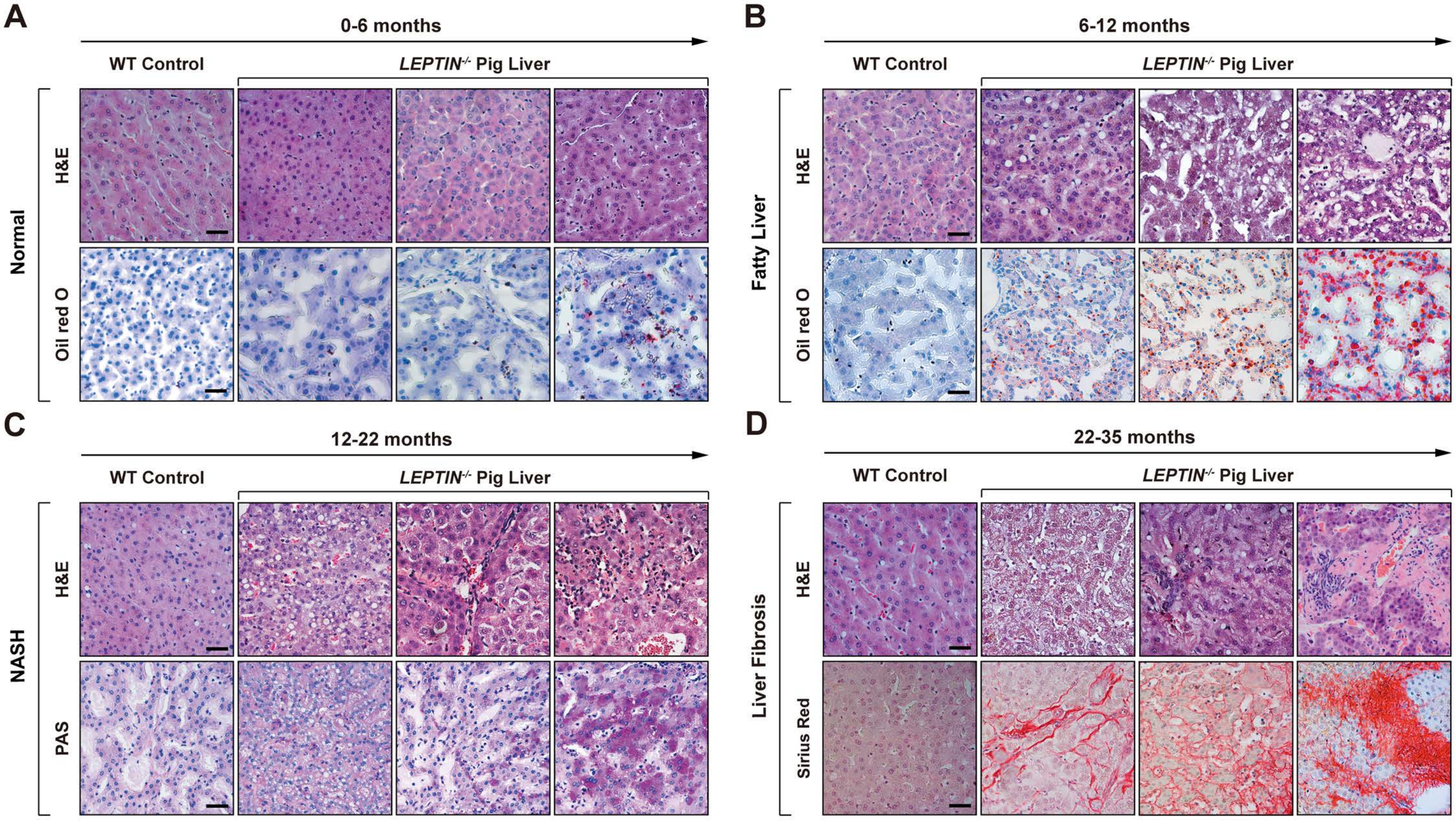
A
0-6 months
WT Control
LEPTIN-/- Pig Liver
Normal
H&E
Oil red O
B
6-12 months
WT Control
LEPTIN-/- Pig Liver
Fatty Liver
H&E
Oil red O
C
12-22 months
WT Control
LEPTIN-/- Pig Liver
NASH
H&E
PAS
D
22-35 months
WT Control
LEPTIN-/- Pig Liver
Liver Fibrosis
H&E
Sirius Red

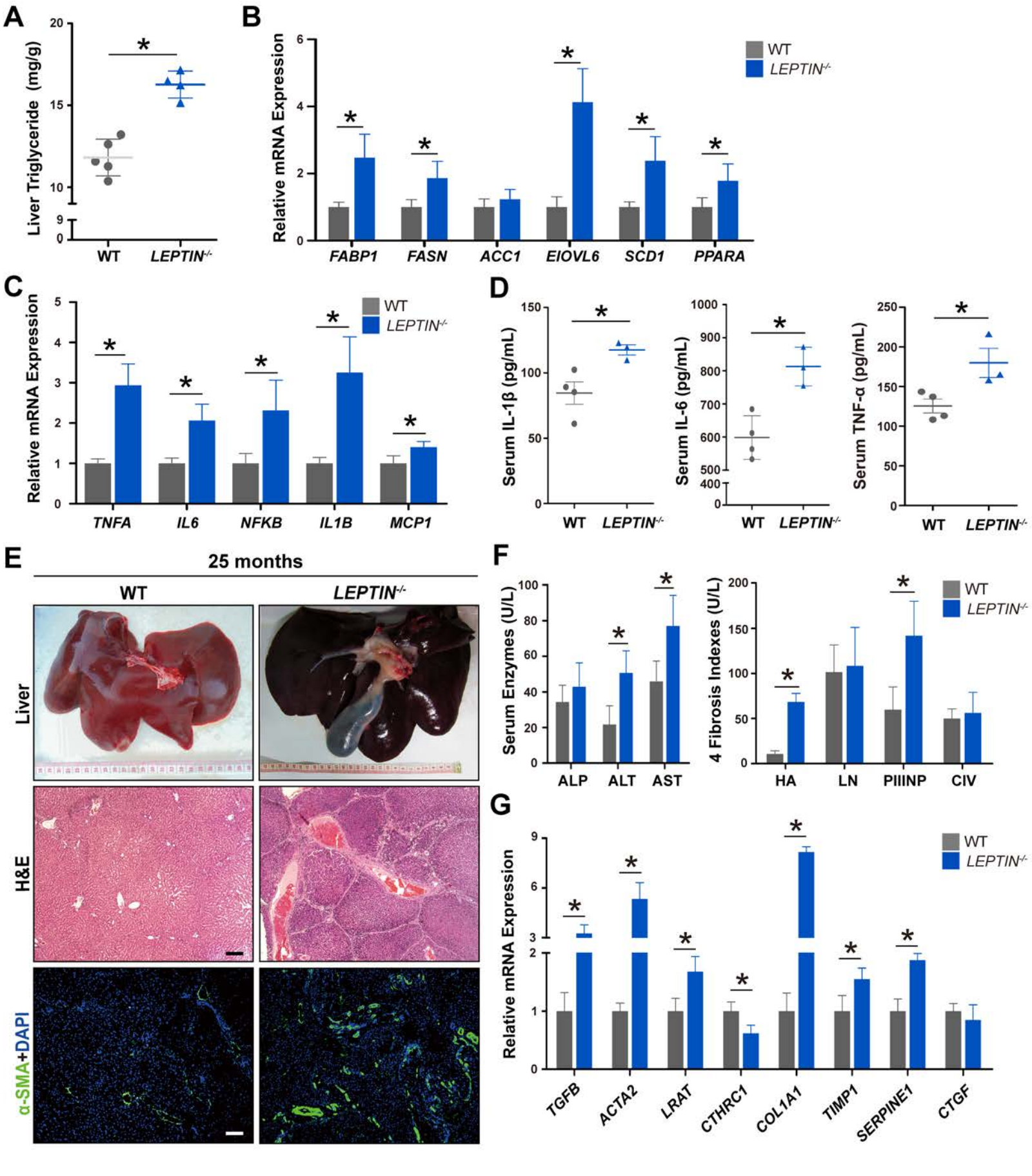
A
Liver Triglyceride (mg/g)
WT
LEPTIN-/-
B
Relative mRNA Expression
WT
LEPTIN-/-
FABP1
FASN
ACC1
EIOVL6
SCD1
PPARA
C
Relative mRNA Expression
TNFA
IL6
NFKB
IL1B
MCP1
D
Serum IL-1β (pg/mL)
Serum IL-6 (pg/mL)
Serum TNF-α (pg/mL)
E
25 months
WT
LEPTIN-/-
Liver
H&E
α-SMA+DAPI
F
Serum Enzymes (U/L)
ALP
ALT
AST
4 Fibrosis Indexes (U/L)
HA
LN
PIIINP
CIV
G
Relative mRNA Expression
TGFB
ACTA2
LRAT
CTHRC1
COL1A1
TIMP1
SERPINE1
CTGF

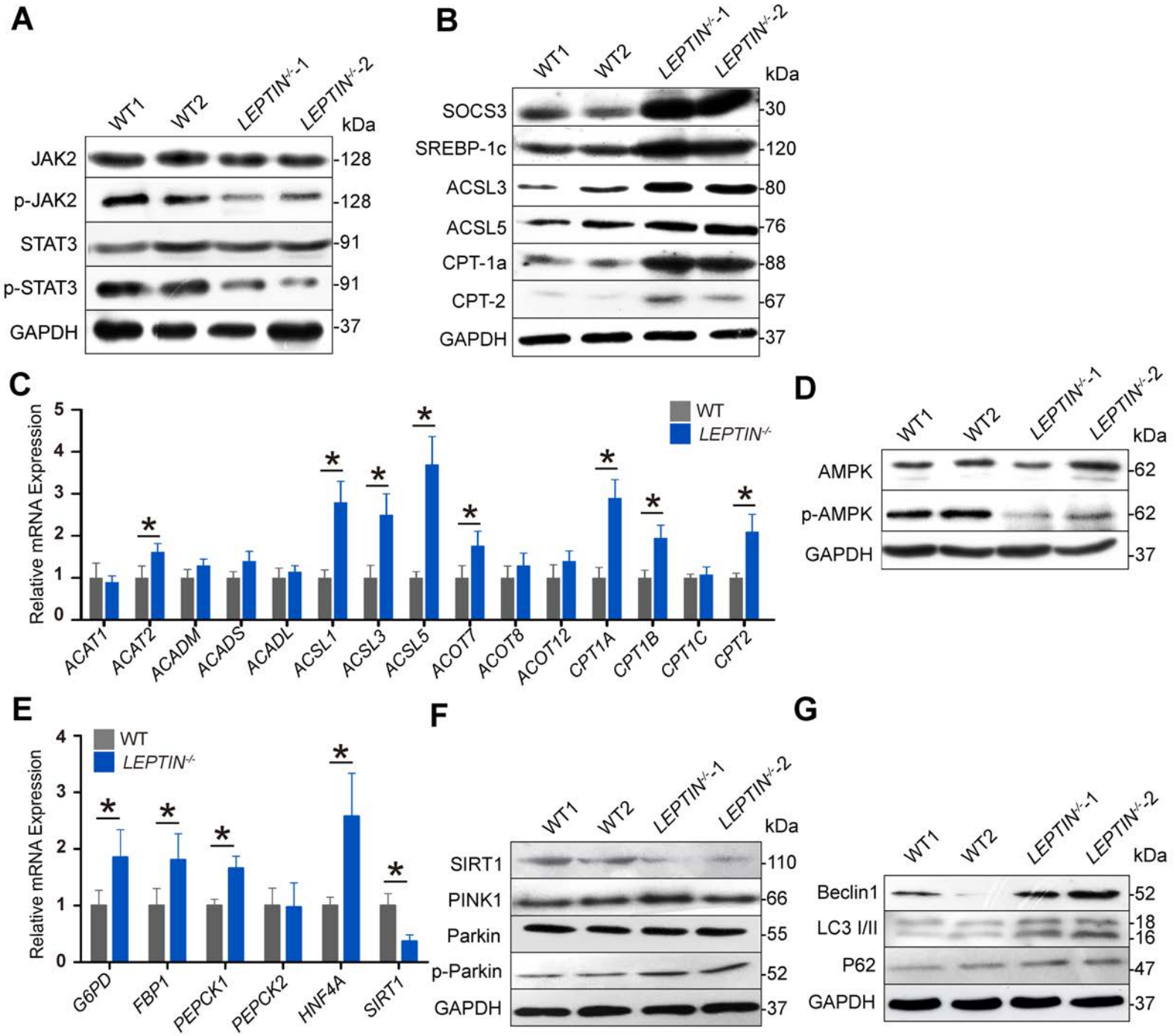
A
WT1
WT2
LEPTIN-/--1
LEPTIN-/--2
kDa
JAK2
p-JAK2
STAT3
p-STAT3
GAPDH
128
128
91
91
37
B
WT1
WT2
LEPTIN-/--1
LEPTIN-/--2
kDa
SOCS3
SREBP-1c
ACSL3
ACSL5
CPT-1a
CPT-2
GAPDH
30
120
80
76
88
67
37
C
Relative mRNA Expression
WT
LEPTIN-/-
ACAT1
ACAT2
ACADM
ACADS
ACADL
ACSL1
ACSL3
ACSL5
ACOT7
ACOT8
ACOT12
CPT1A
CPT1B
CPT1C
CPT2
D
WT1
WT2
LEPTIN-/--1
LEPTIN-/--2
kDa
AMPK
p-AMPK
GAPDH
62
62
37
E
Relative mRNA Expression
WT
LEPTIN-/-
G6PD
FBP1
PEPCK1
PEPCK2
HNF4A
SIRT1
F
WT1
WT2
LEPTIN-/--1
LEPTIN-/--2
kDa
SIRT1
PINK1
Parkin
p-Parkin
GAPDH
110
66
55
52
37
G
WT1
WT2
LEPTIN-/--1
LEPTIN-/--2
kDa
Beclin1
LC3 I/II
P62
GAPDH
52
18
16
47
37

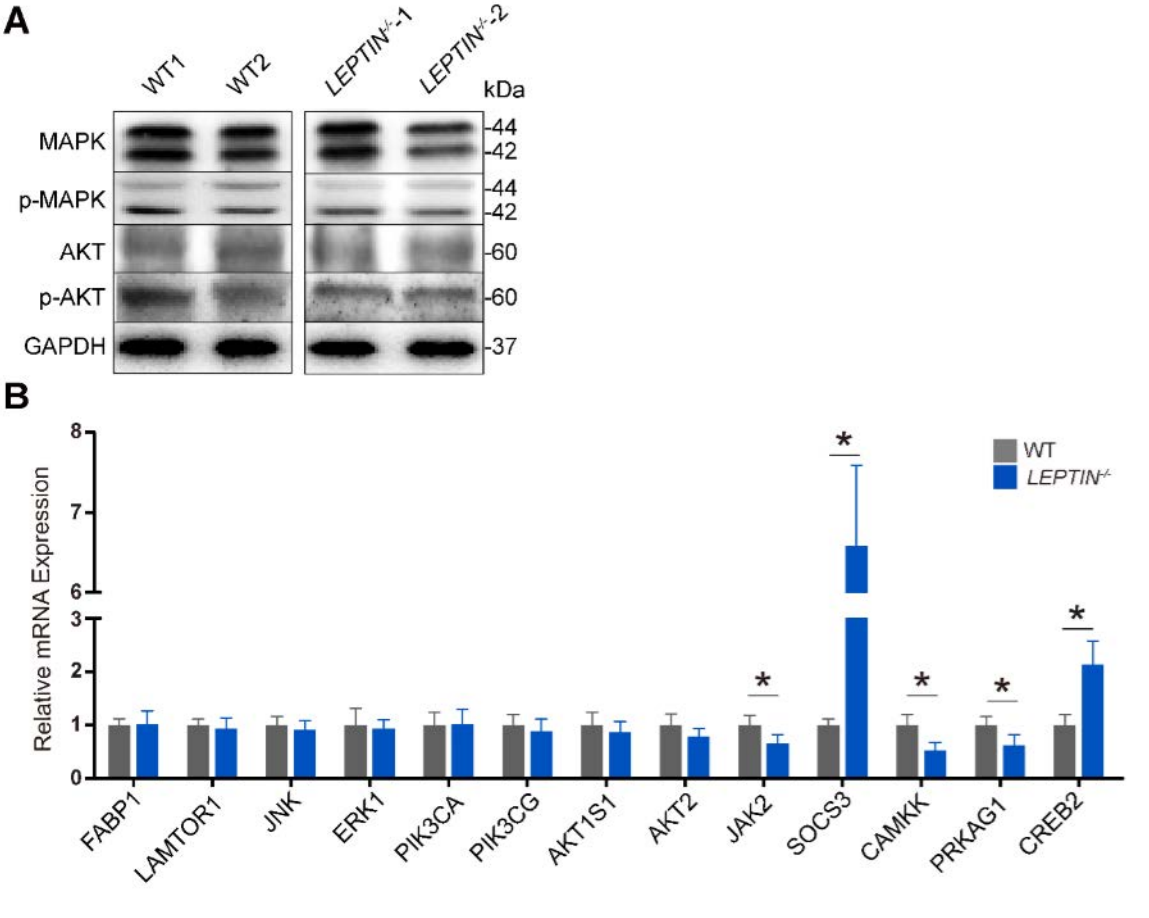
A
WT1
WT2
LEPTIN-/--1
LEPTIN-/--2
kDa
MAPK
p-MAPK
AKT
p-AKT
GAPDH
44
42
44
42
60
60
37
B
Relative mRNA Expression
8
7
6
3
2
1
0
WT
LEPTIN-/-
*
*
*
*
*
FABP1
LAMTOR1
JNK
ERK1
PIK3CA
PIK3CG
AKT1S1
AKT2
JAK2
SOCS3
CAMKK
PRKAG1
CREB2

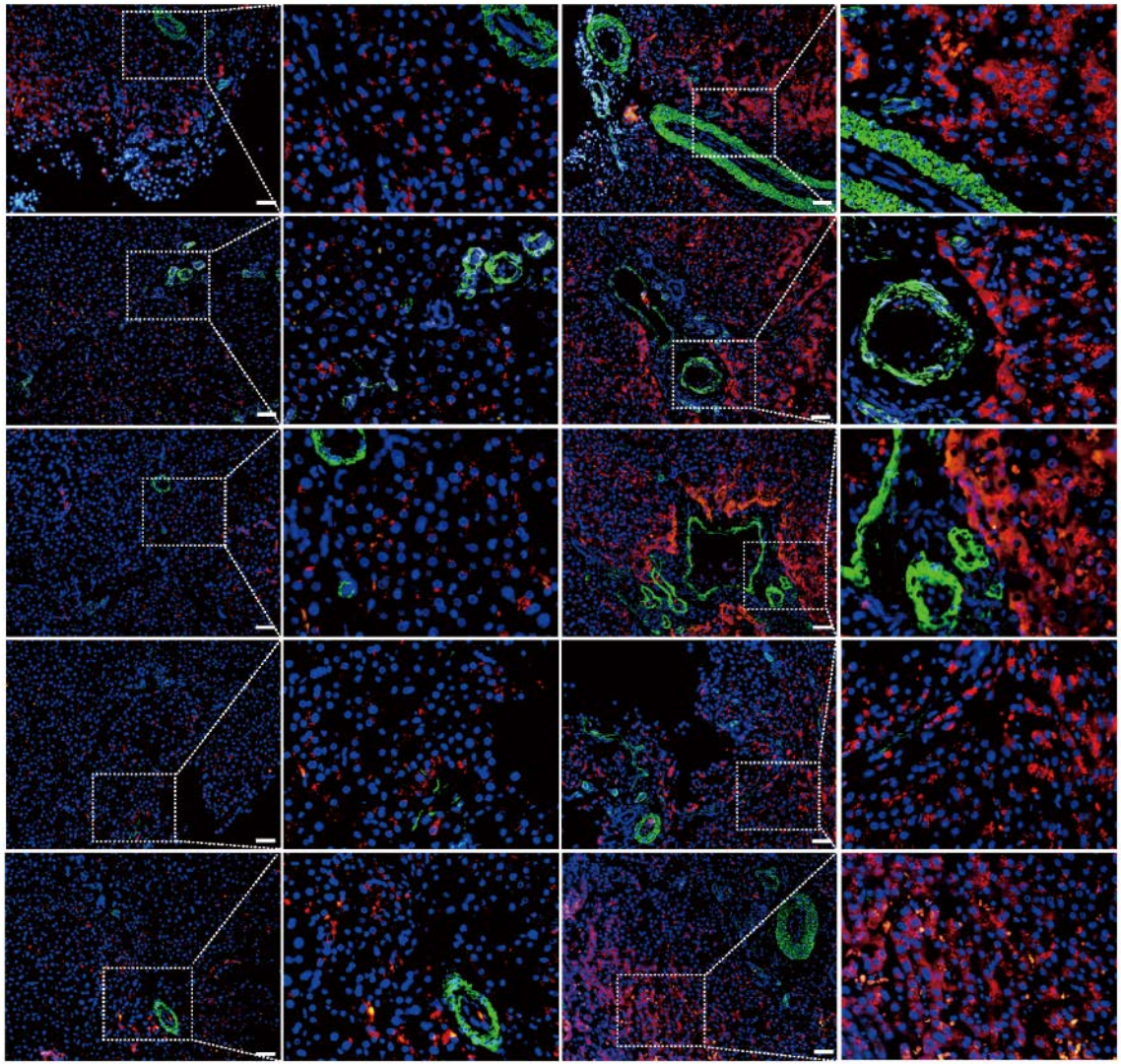
WT Liver
LEPTIN -/- Liver
α-SMA+SOCS3+DAPI
α-SMA+SREBP-1c+DAPI
α-SMA+CPT1a+DAPI
α-SMA+CPT2+DAPI
α-SMA+ACSL3+DAPI

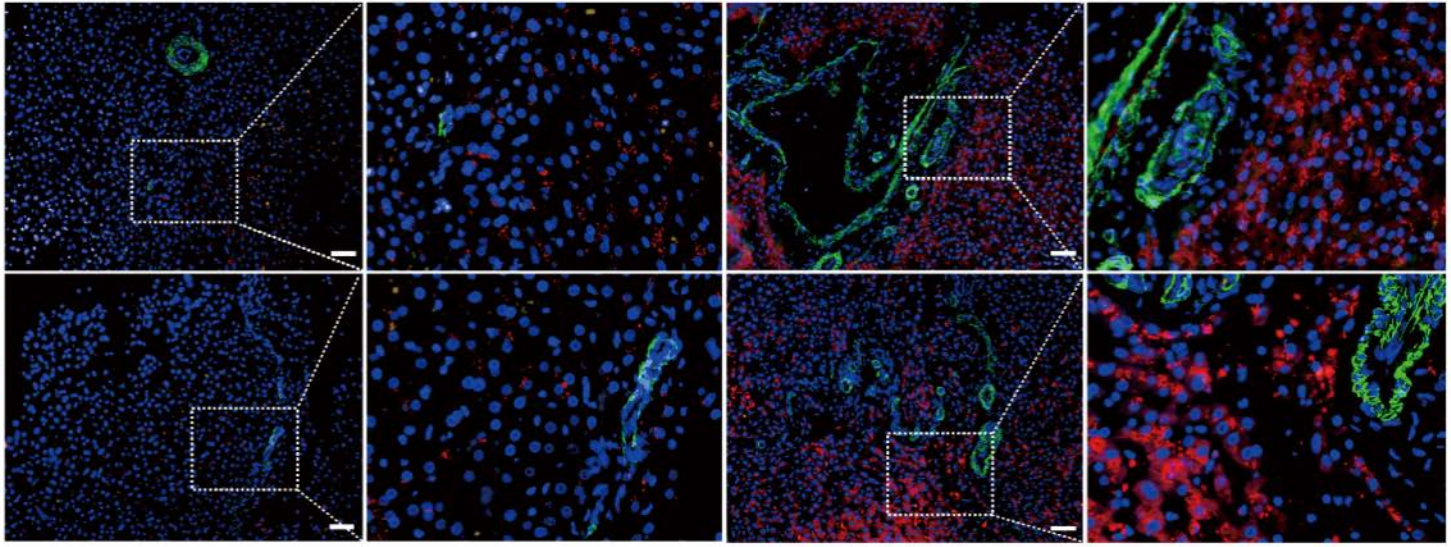
WT Liver
LEPTIN-/- Liver
α-SMA+PEPCK + DAPI
α-SMA+G6pase+ DAPI

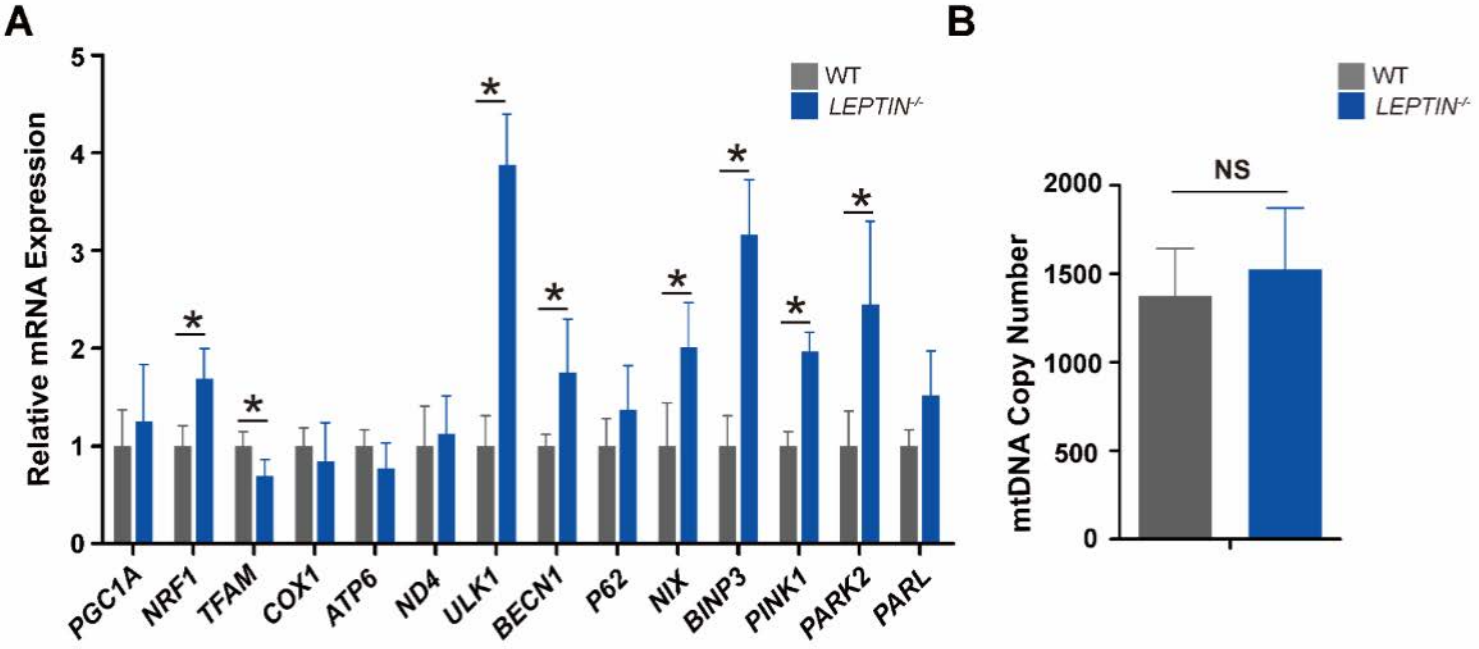
A
Relative mRNA Expression
5
4
3
2
1
0
WT
LEPTIN-/-
*
PGC1A
NRF1
TFAM
COX1
ATP6
ND4
ULK1
BECN1
P62
NIX
BINP3
PINK1
PARK2
PARL
B
mtDNA Copy Number
2000
1500
1000
500
0
NS
WT
LEPTIN-/-

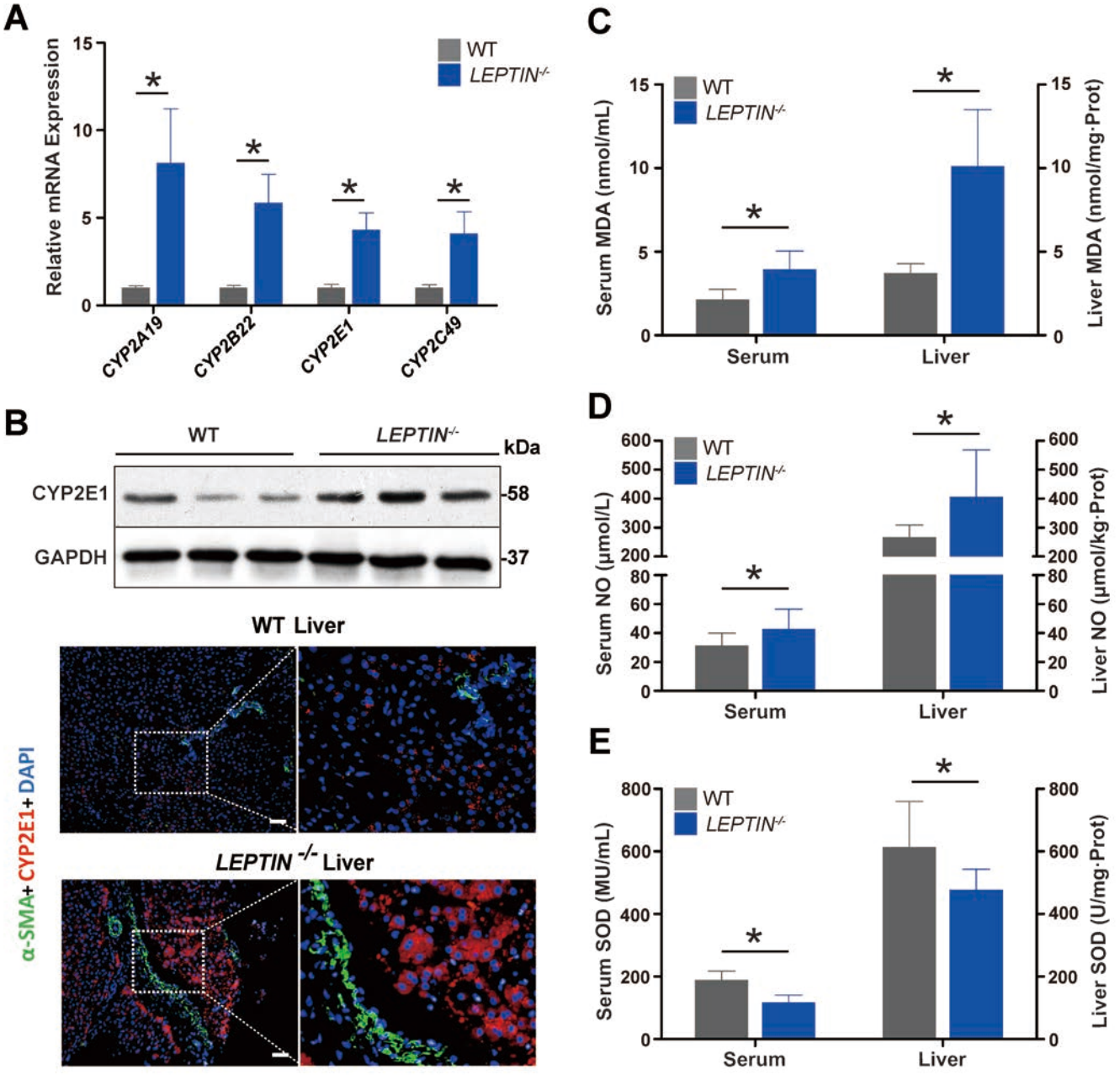
A
Relative mRNA Expression
WT
LEPTIN-/-
CYP2A19
CYP2B22
CYP2E1
CYP2C49
B
WT
LEPTIN-/-
kDa
CYP2E1
GAPDH
58
37
WT Liver
LEPTIN -/- Liver
α-SMA+ CYP2E1+ DAPI
C
Serum MDA (nmol/mL)
Liver MDA (nmol/mg·Prot)
Serum
Liver
D
Serum NO (μmol/L)
Liver NO (μmol/kg·Prot)
E
Serum SOD (MU/mL)
Liver SOD (U/mg·Prot)

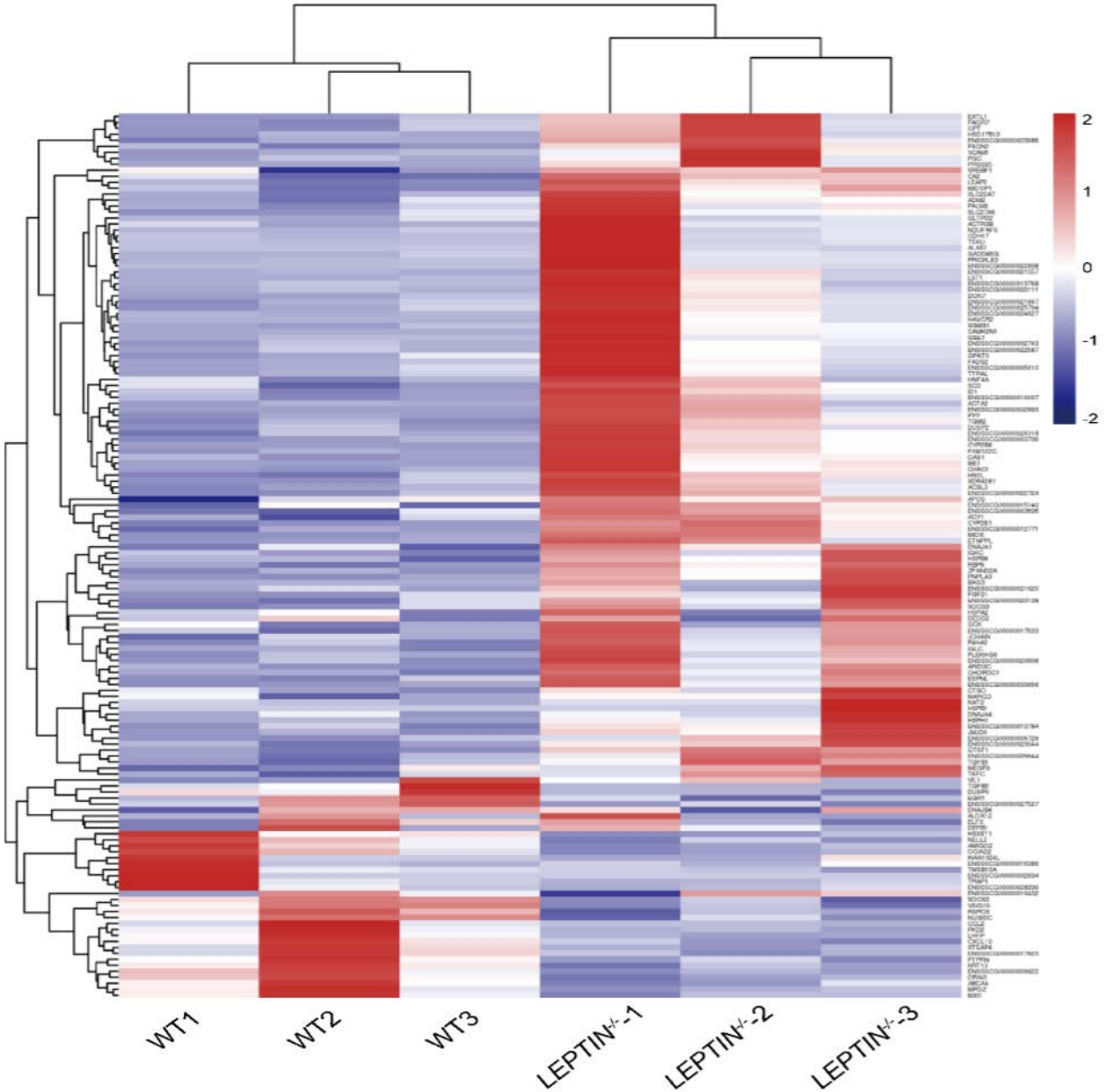
2
1
0
-1
-2
WT1
WT2
WT3
LEPTIN-/--1
LEPTIN-/--2
LEPTIN-/--3

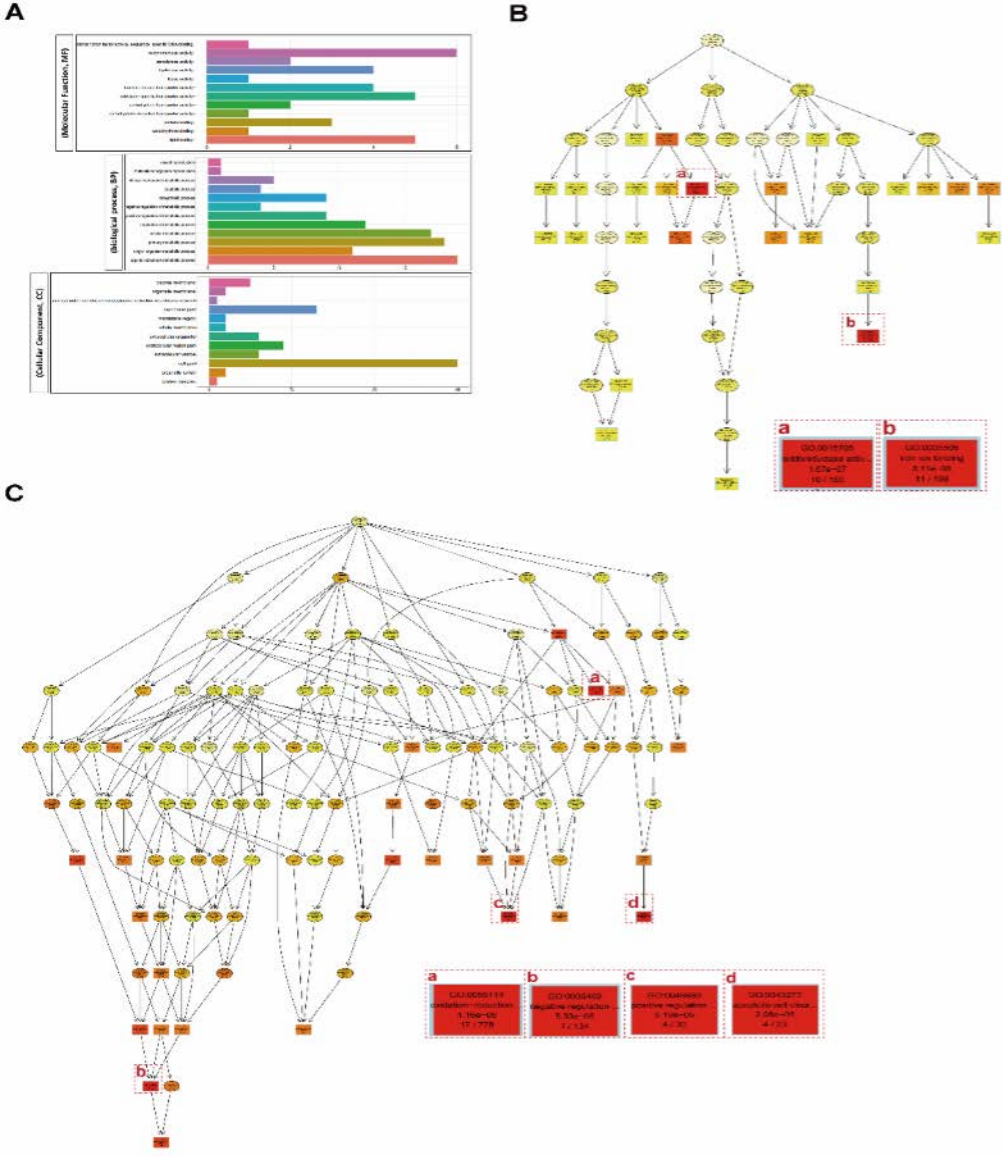
A
(Molecular Function, MF)
(Biological process, BP)
(Cellular Component, CC)
B
a
b
C
a
b
c
d

A

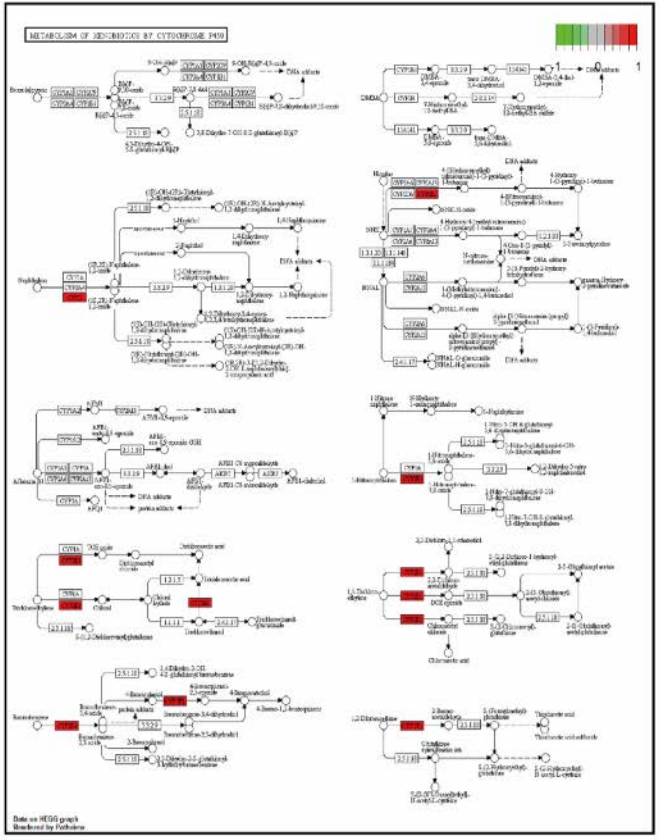
METABOLISM OF XENOBIOTICS BY CYTOCHROME P450
1
Data on KEGG graph
Rendered by Pathview

B

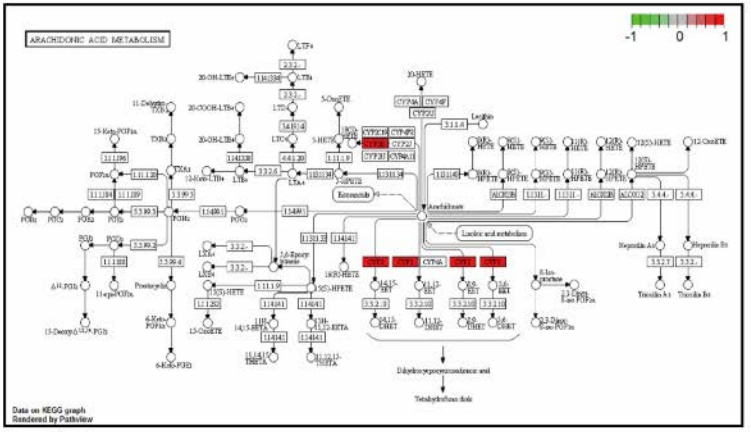
ARACHIDONIC ACID METABOLISM
-1
0
1
Leukotriene and eicosanoid
Lipoxins
Resolvins
Data on KEGG graph
Rendered by Pathview

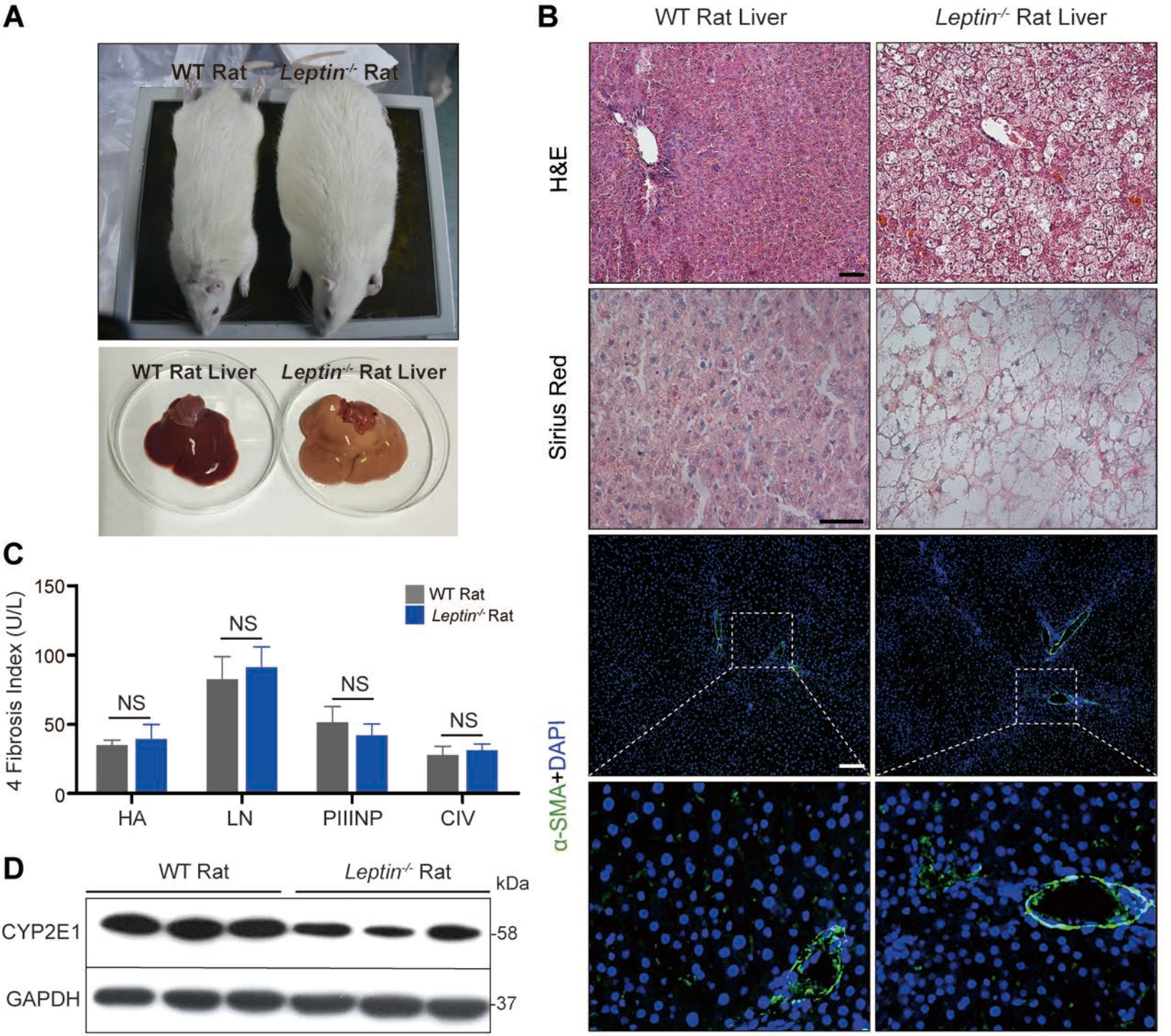
A
WT Rat
Leptin-/- Rat
WT Rat Liver
Leptin-/- Rat Liver
B
WT Rat Liver
Leptin-/- Rat Liver
H&E
Sirius Red
α-SMA+DAPI
C
4 Fibrosis Index (U/L)
150
100
50
0
WT Rat
Leptin-/- Rat
NS
NS
NS
NS
HA
LN
PIIINP
CIV
D
WT Rat
Leptin-/- Rat
kDa
CYP2E1
GAPDH
-58
-37

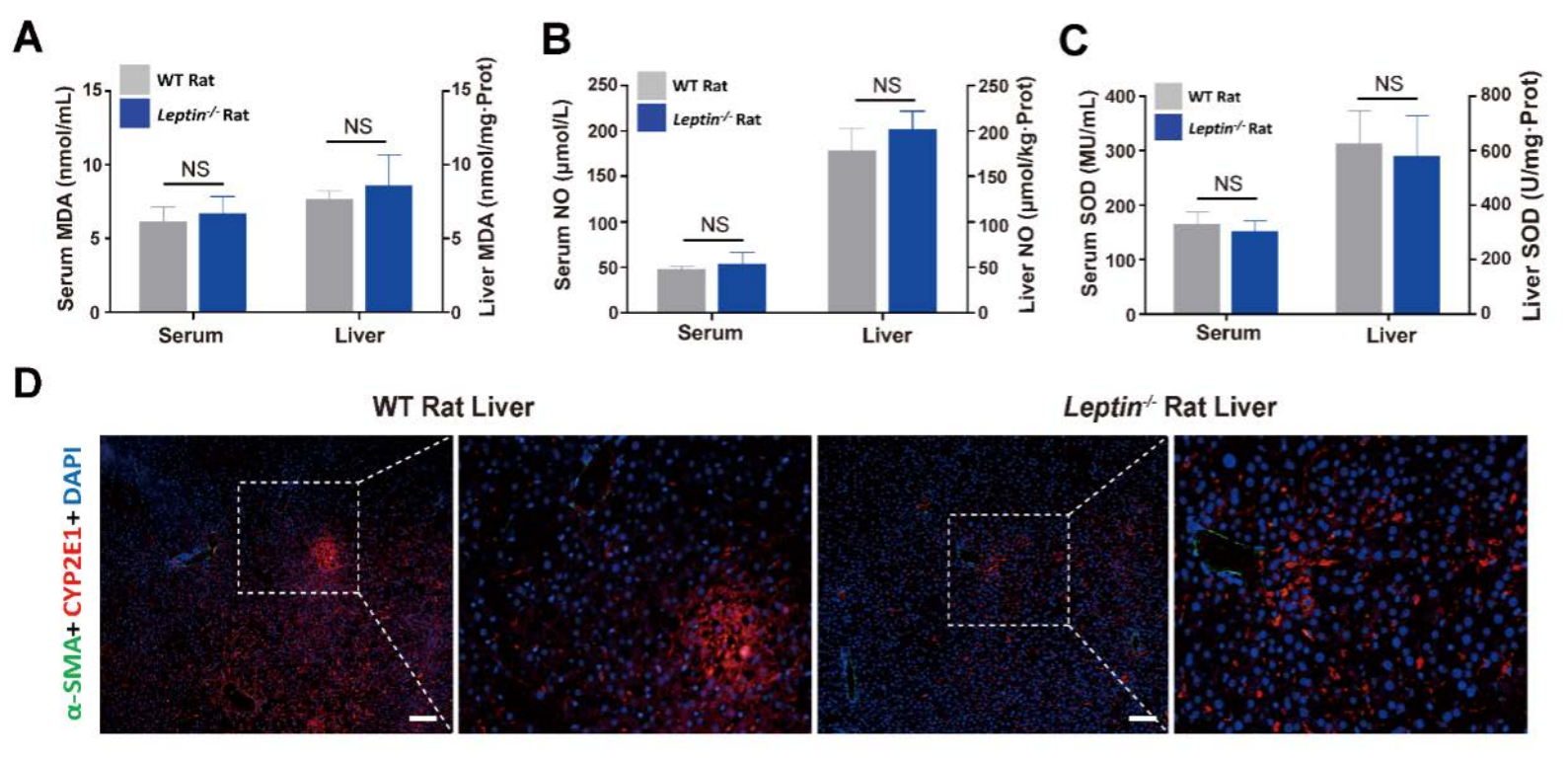
A
WT Rat
Leptin-/- Rat
Serum MDA (nmol/mL)
Liver MDA (nmol/mg·Prot)
NS
NS
Serum
Liver
B
WT Rat
Leptin-/- Rat
Serum NO (μmol/L)
Liver NO (μmol/kg·Prot)
NS
NS
Serum
Liver
C
WT Rat
Leptin-/- Rat
Serum SOD (MU/mL)
Liver SOD (U/mg·Prot)
NS
NS
Serum
Liver
D
WT Rat Liver
Leptin-/- Rat Liver
α-SMA+ CYP2E1+ DAPI

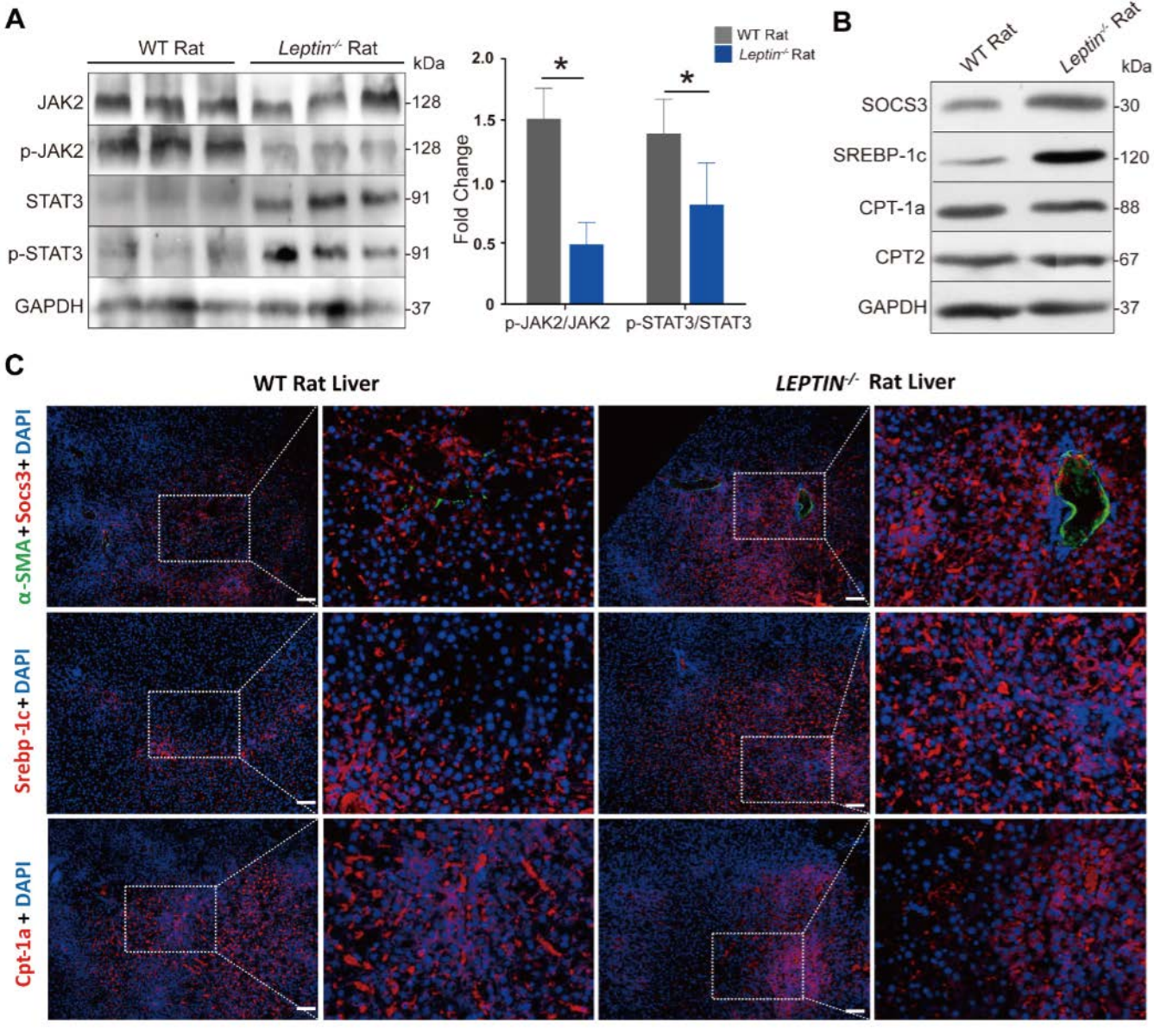
A
WT Rat
Leptin-/- Rat
kDa
JAK2
p-JAK2
STAT3
p-STAT3
GAPDH
128
128
91
91
37
WT Rat
Leptin-/- Rat
Fold Change
2.0
1.5
1.0
0.5
0
*
*
p-JAK2/JAK2
p-STAT3/STAT3
B
WT Rat
Leptin-/- Rat
kDa
SOCS3
SREBP-1c
CPT-1a
CPT2
GAPDH
30
120
88
67
37
C
WT Rat Liver
LEPTIN-/- Rat Liver
α-SMA + Socs3 + DAPI
Srebp-1c + DAPI
Cpt-1a + DAPI

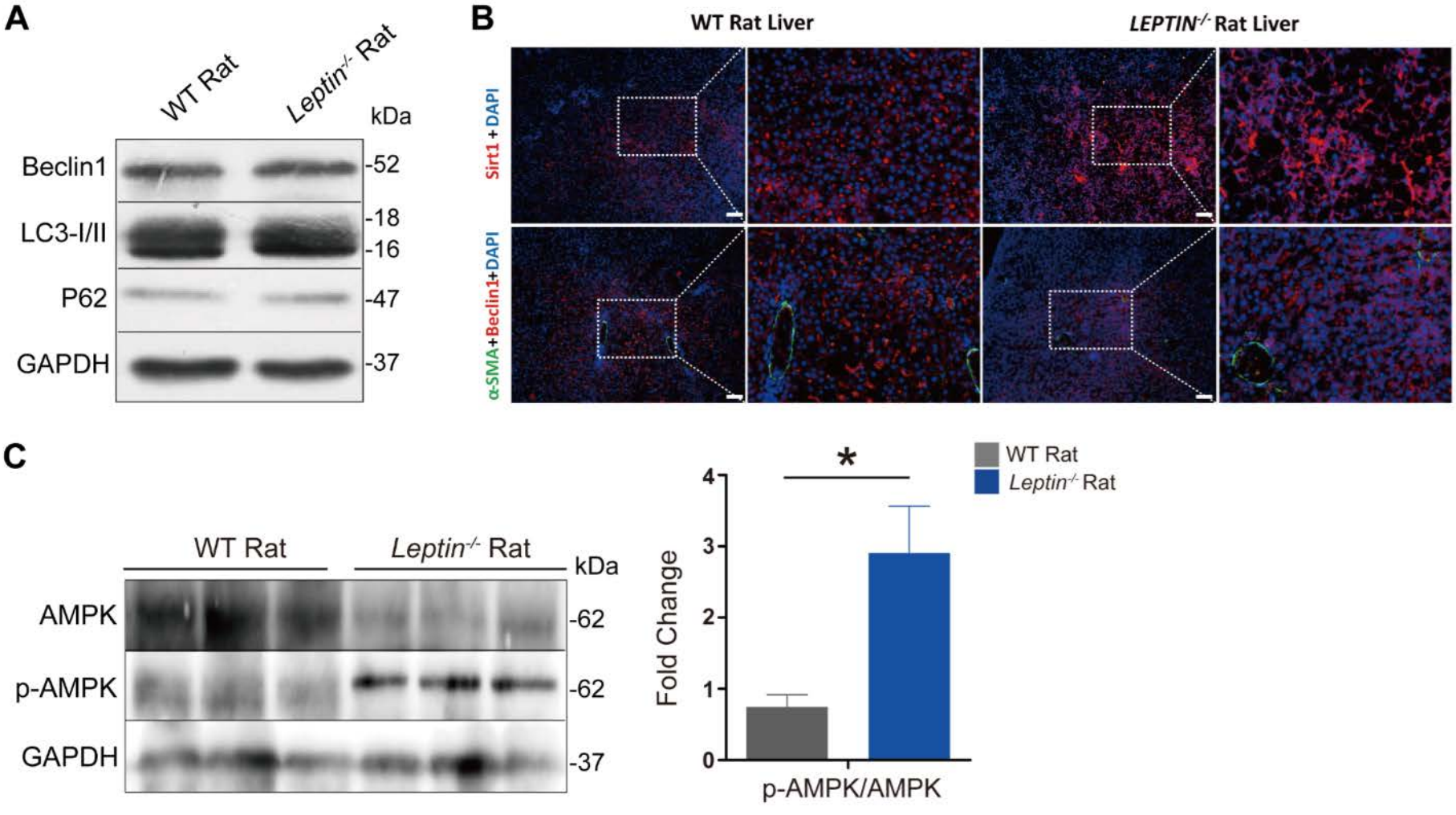
A
WT Rat
Leptin-/- Rat
kDa
Beclin1
-52
LC3-I/II
-18
-16
P62
-47
GAPDH
-37
B
WT Rat Liver
LEPTIN-/- Rat Liver
Sirt1 + DAPI
α-SMA+Beclin1+DAPI
C
WT Rat
Leptin-/- Rat
kDa
AMPK
-62
p-AMPK
-62
GAPDH
-37
*
WT Rat
Leptin-/- Rat
Fold Change
0
1
2
3
4
p-AMPK/AMPK

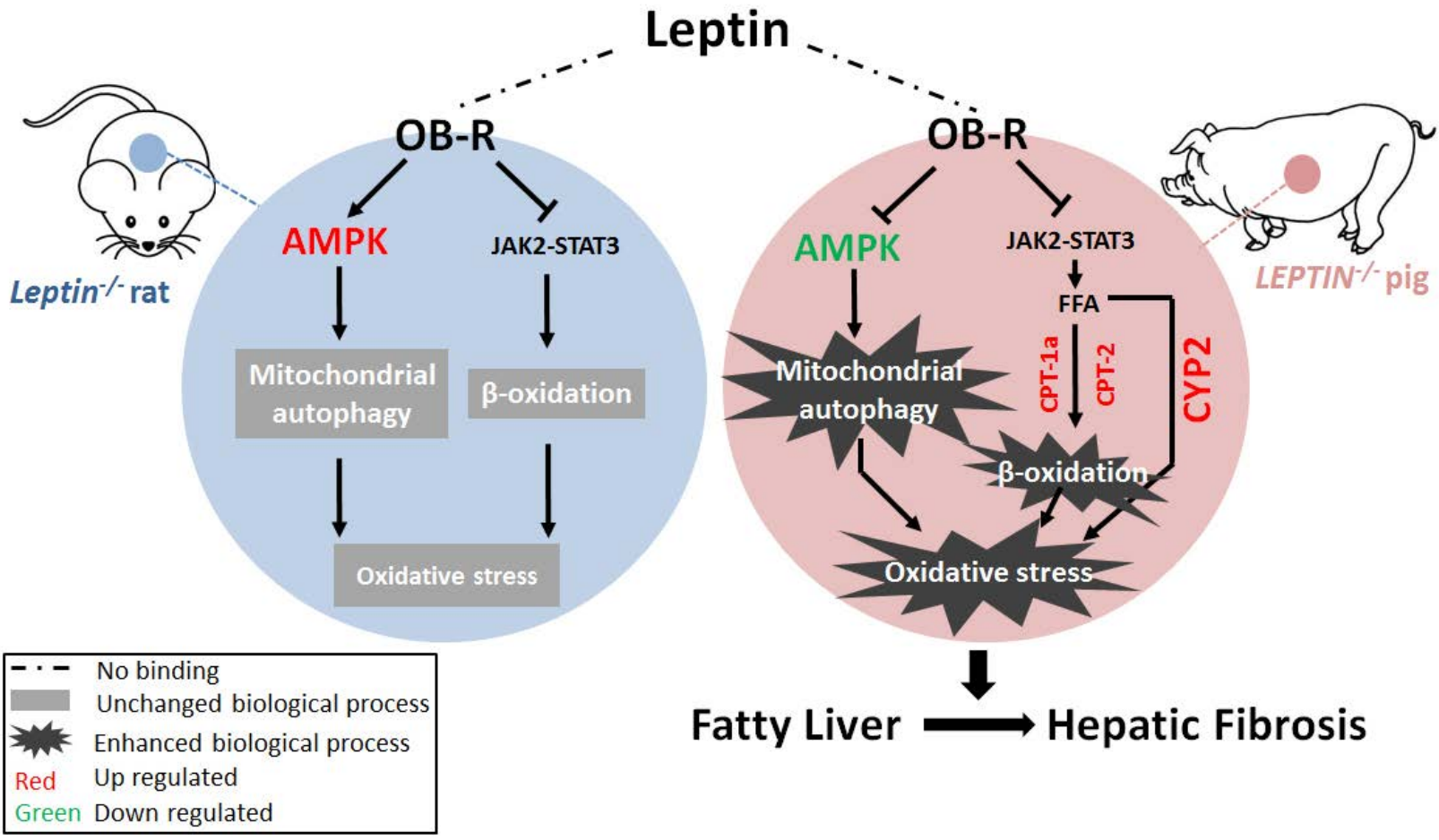
Leptin
OB-R
AMPK
JAK2-STAT3
Mitochondrial autophagy
β-oxidation
Oxidative stress
Leptin-/- rat
OB-R
AMPK
JAK2-STAT3
FFA
CPT-1a
CPT-2
CYP2
Mitochondrial autophagy
β-oxidation
Oxidative stress
LEPTIN-/- pig
No binding
Unchanged biological process
Enhanced biological process
Red Up regulated
Green Down regulated
Fatty Liver
Hepatic Fibrosis

Type of pig	NASH Score (12-22 months)	Fibrosis Score (22-35 months)
LEPTIN$^{-/-}$*-1*	5.43	3.33
LEPTIN$^{-/-}$*-2*	4.66	3.00
LEPTIN$^{-/-}$*-3*	3.33	2.67
Mean ± SD	**4.47 ± 0.86**	**3.00 ± 0.27**
WT-1	0	0.67
WT-2	0.33	0.33
WT-3	0.67	0
Mean ± SD	**0.33 ± 0.27**	**0.33 ± 0.27**